STRUCTURAL AND ELECTRONIC PROPERTIES OF ORGANIC LAYERS ON AU(111)

A Thesis Submitted to
the Graduate School of Engineering and Sciences of
İzmir Institute of Technology
in Partial Fulfillment of the Requirements for the Degree of

DOCTOR OF PHILOSOPHY

in Material Science and Engineering

by
Özlem KAP

June 2018
İZMİR

We approve the thesis of **Özlem KAP**

Examining Committee Members:

_____
Prof. Dr. Canan VARLIKLI
Department of Photonics, İzmir Institute of Technology

_____
Assoc. Prof. Dr. İlbeyi AVCI
Department of Physics, Ege University

_____
Assoc. Prof. Dr. Özgenç EBİL
Department of Chemical Engineering, İzmir Institute of Technology

_____
Assist. Prof. Dr. Burak GÜLTEKIN
Solar Energy Institute, Ege University

29 June 2018

_____
Assist. Prof. Dr. Umut ADEM
Department of Material Science and Engineering
İzmir Institute of Technology

_____   _____
Prof. Dr. Canan VARLIKLI   **Assoc. Prof.Dr. Cem ÇELEBİ**
Supervisor, Department of Photonics,   Co-advisor, Department of Physics
İzmir Institute of Technology   İzmir Institute of Technology

_____   _____
Prof. Dr. Mustafa Muammer DEMİR   **Prof. Dr. Aysun SOFUOĞLU**
Head of the Department of Material Science Dean of the Graduate School of
and Engineering   Engineering and Science

ACKNOWLEDGEMENTS

A very special thanks to my cousins, Seda Kurtoğlu and İzzettin Kürklü for their unconditional support.

I would like to thank Sinem Duman and Tuğba Işık for their valuable help during the preparation of my thesis.

My utmost appreciation goes to Tülin-İsmet Uzkut for being stand-in parents and their unconditional support and love. I always feel their presence on my side.

Most importantly, none of this would have been possible without them, Hülya-Selahattin Kap. They always have a deep love, patience and believe in me. This thesis is dedicated to them, who have given me their unconditional support, both financially and emotionally during my study.

My deepest gratitude goes out to my dear, Michel. It was really nice to follow the signs which made me lucky at the end. We have not spent the years yet but our emotionally closeness is closing the gap. You are always on my side with your supports and helps indeed that involved in this work.

ABSTRACT

STRUCTURAL AND ELECTRONIC PROPERTIES OF ORGANIC LAYERS ON AU(111)

Self-assembled monolayers (SAMs) have attracted attention due to their chemical and structural properties providing numerous new applications such as molecular electronics and electrochemistry. SAMs were optimized by experimental techniques including Scanning Tunneling Microscope (STM), Scanning Tunnelling Spectroscopy (STS), X-Ray Photoelectron Spectroscopy (XPS), Polarization-Modulation Infrared Reflection-Absorption Spectroscopy (PM-IRRAS), Cyclic Voltammetry (CV), Electrochemical Impedance Spectroscopy (EIS).

The first part of this dissertation deals with the dynamic behaviour of decanethiol SAMs. The dynamic behaviour alkanethiols SAM is unique for its configuration giving indirect evidence for the structural ordering within the formation. Structural stability of decanethiol (decanesulfonates) SAMs were investigated by space- and time- resolved STM. Decanesulfonate phase shows less dynamic behaviour and is structurally more stable compared to the decanethiol phases.

The second part of this dissertation describes the binding properties of alkyne molecules adsorbed on gold. Alkyne oxidation occurs at ambient conditions but it is found that unlike thiols, ordered alkyne SAM structure has still chemical bonding between carbon and gold. Alkyne SAMs are good candidates for the ambient molecular electronics application.

The last part of this dissertation presents the study of a monolayer of a Ru(II) complex which is prepared on gold substrate. With the help of STM and XPS methods, the ordered structure and binding properties of the CS28 molecules were characterized by providing a deeper insight into the carboxyl and sulfur groups binding affinity to gold substrate. CV and EIS methods were used to compare the adsorption properties and charge transfer process with the bare gold substrate and SAMs.

ÖZET

ORGANİK KATMANLARIN AU(111) ÜZERİNDE YAPISAL VE ELEKTRONİK ÖZELLİKLERİ

Kendiliğinden düzenlenen tek katmanlı yapılar (SAM), moleküler elektronik ve elektrokimya gibi alanlarda çok sayıda yeni uygulamaya olanak sağlayan kimyasal ve yapısal özelliklerinden dolayı dikkat çekmektedir. Kendiliğinden düzenlenen tek katmanlı yapı, taramalı tünelleme mikroskobu, taramalı tünelleme spektroskopisi, X-Işını fotoelektron spektroskopisi, polarizasyon-modülasyon kızılötesi yansıma emilim spektroskopisi, döngüsel voltammetri, elektrokimyasal empedans spektroskopisi gibi çeşitli deneysel tekniklerle optimize edilmiştir.

Bu tezin ilk bölümü dekantiyolun kendiliğinden düzenlenen tek katmanlı yapısının dinamik davranışı ile ilgilidir. Tek katmanlı alkantiyol yapıların dinamik davranışı, konfigürasyonu nedeniyle önemlidir çünkü oluşum içerisindeki yapı düzeni hakkında dolaylı kanıt sağlar. Dekantiyol ve hava ile okside olmuş dekantiyolün (dekansülfonat) yapısal kararlılığı uzay- ve zaman- çözünürlüklü taramalı tünelleme mikroskopisi tarafından incelenmiştir. Dekansülfonat fazı, dekantiyol fazlarına kıyasla daha az dinamik davranış gösterir ve yapısal olarak daha kararlıdır.

Bu tezin ikinci kısmı, altın üzerine adsorbe edilmiş alkin moleküllerinin bağlanma özelliklerini açıklamaktadır. Alkin oksidasyonu normal şartlarda oluşur, ancak kendiliğinden düzenlenen tek katmanlı yapının tiyollerden farklı olarak, karbon ve altın arasında hala kimyasal bağa sahip olduğu anlaşılmıştır. Alkin tabanlı kendiliğinden düzenlenen tek katmanlar, moleküler elektronik uygulamaları için iyi bir adaydır.

Tezin son kısmı, altın alt katman üzerinde çözelti yöntemiyle hazırlanan bir Ru (II) kompleksi tek tabakasının incelenmesini açıklamaktadır. Taramalı tünelleme mikroskopu ve X-Işını fotoelektron spektroskopisi yöntemleri ile CS28 molekülünün yapı düzeni ve bağlanma özellikleri, karboksil ve sülfür yapıların, altın alt katman üzerinde bağlanma eğilimleri derinlemesine incelenerek ortaya koyulmuştur. Çevrimsel voltametri ve empedans spektroskopisi yöntemleri, altın üzerinde kendiliğinden düzenlenenen tek katmanlı yapının ve boş altın alt tabakanın adsorpsiyon özelliği ve yük aktarım olaylarını kıyaslamak amacıyla kullanılmıştır.

Dedicated to my parents…

TABLE OF CONTENTS

LIST OF FIGURES

LIST OF TABLES

LIST OF ABBREVIATIONS

CAE   constant analyser energy

CV   cyclic voltammetry

DFT   density functional theory

DMF   N,N-dimethylformamide

EAEA   9-(anthracen-9-ylethynyl)-10-ethynylanthracene

EIS   electrochemical impedance spectroscopy

FCC   face-centered cubic

FFT   fast fourier transform

PM-IRRAS   polarization-modulation infrared reflection absorption spectroscopy

SAM   self-assembled monolayer

SE   spectroscopic ellipsometry

STM   scanning tunnelling microscope

STS   scanning tunnelling spectroscopy

TDM   transition dipole moment

TR-STM   time resolved scanning tunnelling microscopy

UHV   ultra-high vacuum

WCA   water contact angle

XPS   x-ray photoelectron spectroscopy

CHAPTER 1

INTRODUCTION

1.1 General

A self-assembled monolayer (SAM, Figure 1.1) is a film consisting of a single layer of molecules that spontaneously arrange themselves on the surface of a substrate into a crystalline structure. The SAMs consist in general of three separate parts; the head group (linking group), the backbone (main chain) and the specific terminal group. The headgroup has a specific affinity owing to its chemical functionality for a certain surface of a substrate (often the surface of a metal substrate). The formation of the self-assembled monolayer lowers the interfacial free energy between the surface of the substrate and the molecular layer. This process is called chemisorption and is often exothermic (San Juan 2013).
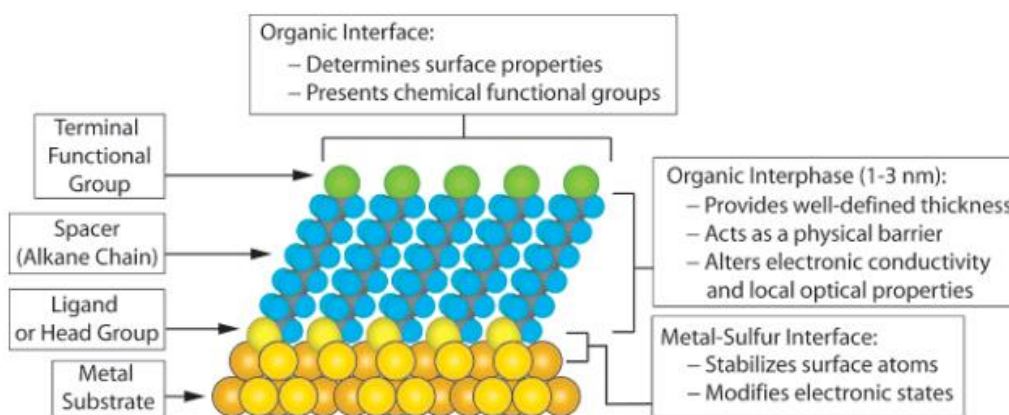
Figure 1.1 Schematic diagram of an ideal n-alkanethiol SAM on a gold (111) surface. The main properties of the SAM are highlighted. Reprinted with permission (Source: Love et al., 2005). Copyright (2005) American Chemical Society

Self-assembled monolayers have become a very effective and promising system for usage in advanced applications in material science, biochemistry, biology, electrochemistry, nanotechnology, molecular electronics, controlling of wettability, corrosion inhibition, protein absorption, lubrication, adhesion and biosensors. The specific binding occurs on well-chosen metal surfaces such as gold, copper, silver,

palladium, platinum and mercury by the specific head groups of the molecules. So far, the most commonly studied SAM is the gold-thiolate (R-S-Au) system because of the strong bonding between the thiols and the gold substrate, which allows highly tunable chemical functionalities. Molecules which have a delocalized π- symmetry are often used as a molecular wire for electronic transport. Aromatic conjugates thiolates are used as molecular wires and it was found that the long-range-ordered wirelike structure exhibit an improved conductivity owing to the small energy gap (Tour et al., 1995). However, these thiol-based SAMs are no so stable against oxidation. This oxidation is enhanced upon irradiation with light leading even to multilayer formation (Hamoudi et al., 2008).

Thermal stability and chemical reactivity are limiting factors for technological applications of self-assembly processes in ambient and aqueous solutions (Vericat, Vela, and Salvarezza 2005). A great advantage of SAMs is that their electronic properties can be tuned by using different specific binding groups, chain lengths and substrates. For that purpose, pyridines, nitriles, isocyanides, disulfides, carboxyclic acid, phosphine, epoxide, arsine specific binding group molecules are used as well as thiols (Bu, Mullen, and Liu 2010).

Anthracene based organic molecules are used for organic electronics, optoelectronics and photochemistry due to their aromatic structure and photoreactivity (Zhao et al., 2008). By using an appropriate UV light wavelength, the anthracene units can be dimerized (polymerized). The photoreactivity of anthracene has been known for over a century, dating back to Fritzsche's isolation of the photodimer in 1869 upon irradiation of the benzene monomer (Fritzsche 1866). Anthracene is a planar, highly aromatic molecule containing three cyclic, fused, benzene-like rings. When illuminated with light at a wavelength of 350 nm, anthracene dimerizes at the 9,10 positions, and this photocycloaddition can be reversed by irradiation at 254 nm (Fox 1999). The structure of the dimer (9,10-dihydrodianthracene) had been postulated as early as 1892 by Linebarger, on the basis of the already-known reactivity of the 9,10 (meso) positions of the central ring of anthracene (Bouas-Laurent et al., 2000). The dimer can be thermally dissociated at elevated temperatures (335-344 °C) in solution or in the solid state (Fox and Wooten 1997). Zareie et al., showed that 2-anthracenethiol and 2-naphtalenethiol SAMs structural rearrange under 254 nm UV light. Anthracene dimers formed by exposing UV light do not oxidize (Zareie, Barber, and McDonagh 2006). Anthracene-2,6-dithioacetate were imaged on a gold (111) surface after exposure to 254 and 365 nm UV light in solution. STM images revealed that irradiation of the molecules at 254 nm leads to dimerization of

the anthracenes, whereas irradiation at 365 nm dissociates the anthracene dimers again (switching behaviour). These applications made the anthracene-based molecules an appealing candidate for molecular electronic applications especially for photoswitching. It should be noted that alkanethiolate SAMs are quite dynamic and exhibit a relatively low conductance, so these SAMs are not the most suitable candidate for molecular electronic applications (San Juan 2013). Van der Waals interactions between neighbouring molecules play a crucial role in the self-assembly process. These forces are much weaker than ionic or covalent bonds (Collard and Fox 1991). The length of the alkyl chains influences the order of the SAMs. Longer alkyl chains exhibit a stronger van der Waals interactions resulting in more stable SAMs than the shorter alkyl chains based SAMs. For instance decanethiol molecules exhibit a two-level switching at room temperature when the molecules are adsorbed on a Au(111) substrate (Wu et al., 2013).

Stability of a SAM monolayer is of great relevance for those who are interested in potential applications of self-assembled monolayers. The carbon-gold SAM system has received the most attention over the last few decades.

In this thesis we will mainly focus on the sulfur-gold and C-gold bonded systems. The experimental techniques that have been used in this study will be introduced and discussed in the second chapter. In chapter 3 we have studied a new phase of the alkanethiol SAM that occurs after prolonged exposure to air. The stability and structure of the alkanethiol monolayer is altered by the oxidation product of the decanethiol, the decanesulfonate. We have studied the oxidation process of self-assembled alkanethiol monolayers on gold using scanning tunneling microscopy and X-ray photoelectron spectroscopy. X-ray photoelectron spectra of the S 2p, O 1s and C 1s core levels have been measured for a fresh SAM and an air-exposed SAM. Air-exposed SAMs oxidize, as can be determined by a shift of the S 2p peak and the appearance of O 1s photoelectrons. The decanesulfonates are arranged in a lamellae-like structure. The herringbone structure of the Au(111) surface is preserved, indicating that the interaction between the molecules and the surface is rather weak. These findings are substantiated by density functional theory calculations. Chapter 4 has been focused to understand the binding properties of the alkyne groups to the Au(111) surface. We conclude that the alkyne oxidation occurs at ambient conditions, but the ordered structure still exhibit chemical bonding between the carbon atoms of the molecule and the gold atoms of the substrate. A Ru(II) complex have been studied on Chapter 5 to investigate the ordered structure and binding properties.

CHAPTER 2

EXPERIMENTAL TECHNIQUES

2.1. Scanning Tunneling Microscope(STM)

The scanning tunneling microscope was invented by Binnig and Rohrer in 1981 at IBM Zurich for which they received the Nobel Prize in 1986 (Binnig et al., 1982). The scanning tunneling microscope (STM) allows to image single atoms and molecules. The principle of STM relies on quantum mechanical tunneling between a sharp metal tip and a conducting surface. In order to achieve tunneling currents in the range of pA to nA the distance between tip and surface should be less than 1 nanometer. These properties make the STM an unique instrument to investigate structural and electronic properties (e.g. local density of states) of surfaces with a high spatial resolution.
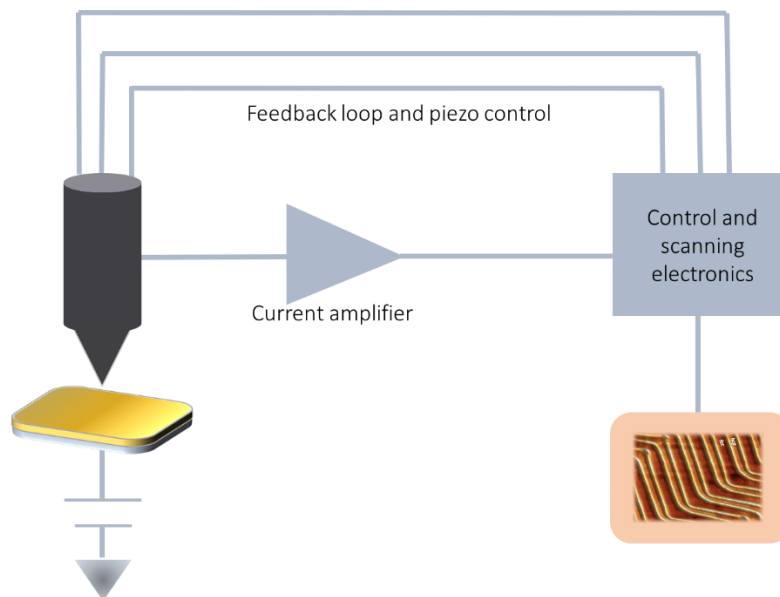
Figure 2.1. Schematic representation of an STM. An atomically sharp tip is positioned about 1 nm away from a surface. A sample bias is applied between tip and substrate resulting in a small tunneling current. The tunneling current is kept constant via a feedback system. The displacement of the tip is recorded as a function of the lateral position.

This novel technique paves the way to other scanning probe microscopy techniques, such as atomic force microscopy where the force between substrate and tip (cantilever) is used to image the surface. An atomically sharp tip is mounted on a xyz-piezoelectric transducer. The feedback electronics is connected to the z-displacement of the piezoelectric transducer and is adjusted in such a way that the tunneling current remains constant, whereas the x- and y-component of the piezoelectric transducer are used for scanning the surface of the sample (see Figure 2.1).

The separation between the tip and substrate is so small that the wavefunctions of tip atoms and surface atoms overlap. If a small bias is applied across the tunneling junction electrons can tunnel from tip atoms to surface atoms or vice versa.

The tunneling current, in its simplest form, is given by the Simmons equation (Wiesendanger 1994),

$$I \propto \frac{V\rho}{z} e^{-\kappa z} \tag{2.1}$$

where I is the tunneling current, V the applied bias voltage, ρ the density of states, κ the inverse decay length and z the tip- sample separation distance. The tunneling current depends exponentially on the tip-sample distance and inverse decay length (see Equation 2.1).

There are two modes of STM operation: the so-called constant current and constant height modes. In the constant tunneling current the feedback loop keeps the tunneling current constant by changing the tip-sample distance z. The z-piezo regulation voltage which keeps the tunneling current constant reflects the topography of the surface. In the constant height mode, the z-piezo voltage is kept constant, while the tunneling current is measured. The constant height mode can only be applied for very flat substrates since the probability of a tip crash is huge.

2.1.1. Scanning Tunneling Spectroscopy (STS)

The STM is a very powerful technique for imaging conductive surfaces down to the atomic level. Single atom imaging is possible with a spatial resolution of about 0.1 nm and a vertical resolution in the picometer (pm) range. Additionally, STM is also able to provide chemical, electronic and dynamical information by employing several

spectroscopic modes. Current-voltage (I-V), current-distance (I-z), inelastic electron tunneling (IETS) and current-time (I-t) spectroscopy techniques are the most well-known spectroscopic STM techniques.

2.1.2. Current-voltage Spectroscopy (I(V) Spectroscopy)

Current-voltage spectroscopy is the most used spectroscopic tool and determines the electronic properties of the surface. The current (I) is recorded when the voltage (V) is ramped from a start voltage to a end voltage in incremental voltage steps. The tip-sample distance is constant during the measurement by deactivated the feedback loop. The curves always collapse at the setpoint, defined by the setpoint current and the start bias voltage before the feedback loop is disabled. The measured current values are therefore relative to the setpoint current and bias voltage: this comprises an important experimental detail that should always be considered when comparing STS data. Metals have a linear I-V curve with a non-zero slope at zero bias, while semiconductors show no current in the band gap region. Numerically calculation of the I-V is gives the differential conductance ($\frac{dI}{dV}$), which is proportional to the density of states.

I(V) spectroscopy is used to determine the local density of states (LDOS) of the surface by the normalized differential conductivity $\frac{dI/dV}{I/V}$, which provides information on the electronic and chemical properties of the sample. At negative sample bias, electrons tunnel from the surface to the tip, which allows to investigate the LDOS of the filled states; while at positive sample bias the electrons tunnel from the tip into the sample allowing one to investigate the LDOS of the empty states of the samples.

2.1.3. Current-distance Spectroscopy (I(z) Spectroscopy)

Since the tunneling current depends exponentially on the bias voltage as well as the tip-substrate separation one can also measure the tunneling current as a function of the tip-sample distance, while keeping the bias voltage constant (I(z) spectrocopy). As is immediately evident from equation 2.1 the inverse decay length can be extracted from the dI/dz signal. Since the inverse decay length is proportional to the square root of the

tunnelling barrier (i.e. the work function) this method allows to make spatial maps of the workfunction.

2.1.4. Current-time Spectroscopy (I(t) Spectroscopy)

The STM can also be used to study dynamical processes on surfaces with high temporal resolution. This method is simple, but very elegant. The STM tip is positioned at a pre-defined position, the feedback loop is disabled and subsequently the tunneling current is recorded as a function of time. The time resolution that can be obtained with this technique is of the order of microseconds and is in principle set by the bandwidth of the IV converter, which is typically of the order of 100-500 kHz.

2.2. X-Ray Photoelectron Spectroscopy (XPS)

X-Ray photoelectron spectroscopy which is referred to as Electron Spectroscopy for Chemical Analysis (ESCA) is a well-known technique to determine the chemical composition of surfaces. Kai Siegbahn, a Swedish physisist, obtained the Nobel prize in 1981 for developing this technique which relies on the photoelectric effect. The kinetic energy of the emitted electrons are measured by using the monochromatic X-rays to obtain information on the inner-shell electrons. The emitted electrons originate from the near-surface region. The process is depicted on Figure 2.2. The information depth depends on the exact energy of the electrons and typically varies from about 1 nm to 10 nm. The electrons are excited by an X-ray source, usually an Al Kα (1486.6 eV) or a Mg Kα (1253.6 eV) source. When a sample is exposed to these X-rays, electrons are emitted from the core levels. The kinetic energy of the emitted photoelectron is the energy difference between the X-ray photon energy hv and the binding energy (BE) of the core level electron. These BE values are fingerprints for the chemical components.

XPS is a very powerful technique for qualitative analysis of the chemical elements of a substrate. In addition, chemical shifts of the BE energies provide valuable information on the exact chemical state of the elements. All the elements are in principle detectable by the XPS method except hydrogen and helium.

XPS is a very powerful technique to study the chemical composition as well as the binding of SAM. (Laibinis et al., 1991).

7
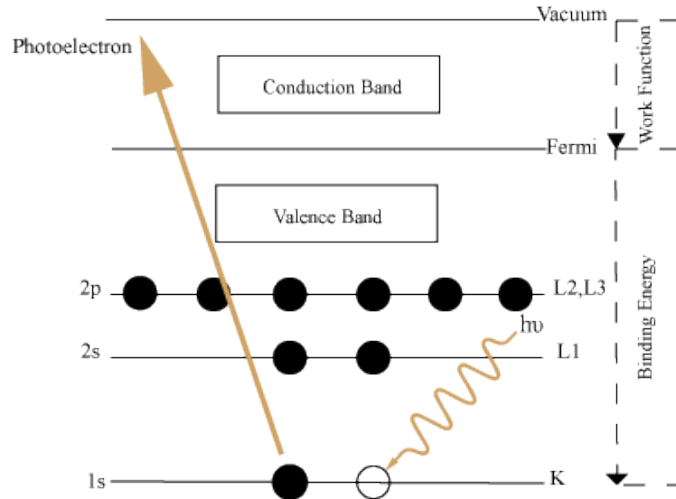
Figure 2.2. Schematic representation principle of X-Ray photoelectron spectroscopy

$$KE = h\nu - BE - \phi_S \tag{2.2}$$

2.3. Spectroscopic Ellipsometry (SE)

Ellipsometry is an optical technique that can be used to determined optical constants, chemical composition, anisotropy, uniformity, crystallinity and thickness of films (Roncali et al., 2010). It is very sensitive characterization method which is able to measure the change in the polarization state of the light by light reflection or transmission. A light beam is reflected by or transmitted through a surface or interface between two media with different refractive indices. The reflected or transmitted light beam is subsequently collected by a detector. Ellipsometry measures the amplitude ratio (ψ) and phase difference (Δ) between in-plane of incidence (p polarization) and perpendicular to this plane (s polarization) polarized light waves. These differences in amplitude and phase are given by the (complex) Fresnel reflection coefficients, r_p and r_s, for the p and s polarizations, respectively. The ratio of these coefficients, ρ, gives the amplitude ratio and phase difference of light from reflection (Wasserman et al., 1989).

Using optical interference, the exact thickness of a film can be determined (Fujiwara 2007). In order to achieve an optimal sensitivity an angle of incidence of about 75°-80° is chosen (Passaglia, Stromberg, and Kruger 1964). The vast majority of SE experiments are carried out in the ultraviolet/visible range; however, SE experiments are

sometimes also performed in the infrared range (Meuse 2000). Figure 2.3 represents ellipsometry measurement principle schematically.
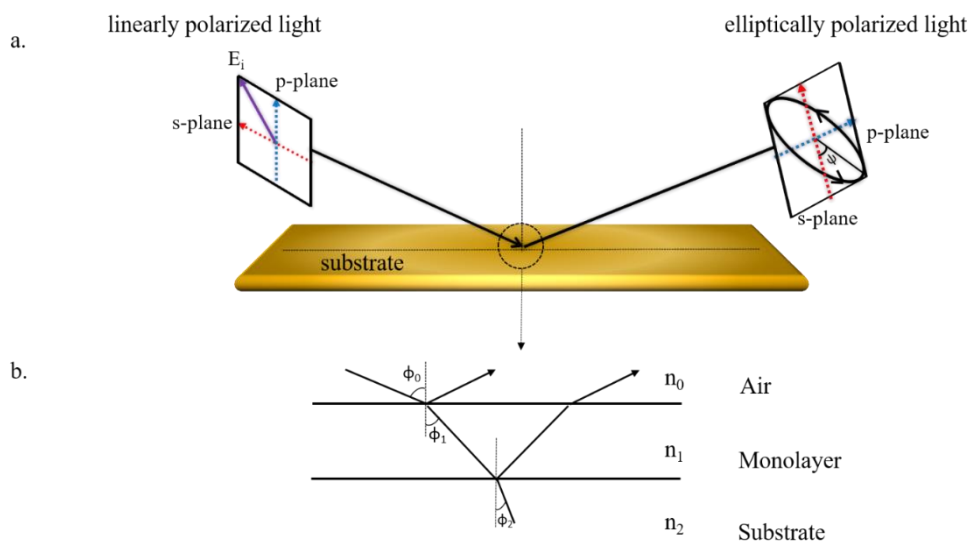
Figure 2.3. (A) Schematic representation of a spectroscopic ellipsometry set-up. Linearly polarized incident light is converted into elliptically polarized light upon reflection from the SAM-substrate system. (B) Two-layer model of the SAM-substrate system.

2.4. Water Contact Angle (WCA)

The surface properties, such as wetting properties, surface-free energy, uniformity and surface order of the SAM-substrate can be determined using contact angle measurements (Ulman 2013). Particularly wettability is an important property of organic surfaces (Laibinis et al., 1991). The contact angle measurement provides quantitative information on the wetting of a solid surface by a liquid droplet. A three-phase equilibrium is established between the liquid surface tension (γ_{LV}), the solid surface tension (γ_{SV}) and the liquid-solid interfacial tension (γ_{SL}). This equilibrium is described by Young's equation;

$$\gamma_{SV} = \gamma_{LV}.\cos\theta + \gamma_{SL} \tag{2.3}$$

9

The most common technique to measure contact angle is the sessile drop method in which the droplet is settled on the solid surface using a syringe. (Clegg et al., 1999). An ordinary goniometer contains a horizontal stage where the sample is mounted between a light source and a CCD camera. The WCA is determined by drawing the tangent line of the droplet. The advancing (θ_a) and receding (θ_r) contact angles, which are measured at the back end and at the front end of the drop respectively, give the maximum and minimum angles between the liquid-substrate interface. The difference between the advancing and receding contact angles is defined as hysteresis (Ulman 2013). A SAM-substrate system that exhibits a small hysteresis is an indication of a well-ordered SAM. Figure 2.4(A) and Figure 2.4(B) show the contact angle measurements on the bare substrate and SAM-substrate, respectively.

A WCA smaller than 90° refers to a hydrophilic surface. SAMs with a polar head group, such as a hydroxyl or a carboxyl, are hydrophilic (Cooper and Leggett 1999). A WCA larger than 90° implies that the surface is hydrophobic. Alkanethiol-based SAM have an apolar methyl (-CH$_3$) head group and are therefore hydrophobic. These hydrophobic SAMs usually have a low surface free energy (Wang et al., 2015). In case that the WCA is larger than 150° we refer to the system as being superhydrophobic (Song et al., 2009). The exact value of the contact angle of a SAM depends on the shape, size, length of the chains as well as the end group of the SAM. The contact angle decreases with decreasing alkane chain length (Ulman 1996).
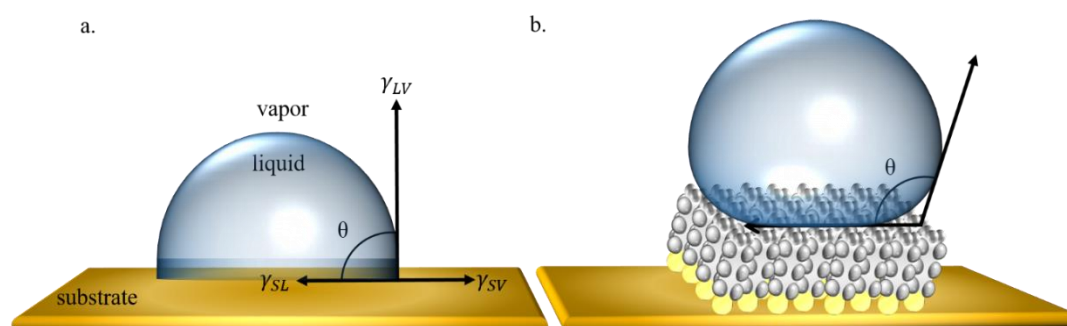
Figure 2.4. (A) Schematic representation of a liquid drop on a bare substrate. The various surface and interface tension are indicated. (B) Schematic presentation of a liquid droplet on a SAM-substrate system.

2.5. Polarization Modulation Infrared Reflection-Absorption Spectroscopy

Polarization modulation infrared reflection-adsorption spectroscopy (PM-IRRAS, PM-IRAS or PM-RAIRS) is an optical technique that can be used to probe the functional groups, substrate- molecule chemical bonds and the orientation of molecules on surfaces (Ramin et al., 2011). In infrared reflection-absorption spectroscopy the reflectance spectrum of a substrate is measured.

The sensitivity and surface selection rules of this technique allows a detailed structural and spectroscopic characterization of a SAM/substrate system. (Rajalingam et al., 2010). Infrared light induces vibrational transitions in molecular bonds, and by measuring the frequency and intensity of the absorbed infrared light, information such as chemical environment, structure, and functional group identity can be elucidated. Infrared radiation is directed from the source through a series of mirrors towards the surface of material under scrutiny. The impinging photons interact with the surface molecules and reflect from the crystal substrate. The reflected beam is directed and focused into the detector through series of mirrors.

2.6. Experimental Setup

SAMs have been studied by a large arsenal of surface science techniques. STM and AFM provide a real-space image of the surface with a high spatial resolution. Usually STM achieves a higher spatial resolution, therefore, the primary tool to study the SAMs is STM. We have used a dedicated ultra-high vacuum RHK STM as shown in Figure 2.5.

The RHK UHV 3000 STM system includes of the following components. A loadlock for quickly introducing new samples and tips without breaking the vacuum and a main chamber which houses the STM. The base pressures of the main chamber and load lock are 1×10^{-10} mbar and 1×10^{-9} mbar, respectively. The main chamber is pumped by an ion pump equipped with a titanium sublimation pump, while the loadlock is pumped by a turbo pump. The scanner, which is of the beetle type, is thermally and mechanically very stable. The scanner piezo is positioned on top of the sample while the three outer piezos are positioned on the ramp of the sample holder. The coarse approach is realized by a stick and slip motion process of the three outer piezos on the ramp of the sample

holder. The sample can be heated either resistively or via a filament. The sample can also be cooled with a flow cryostat.
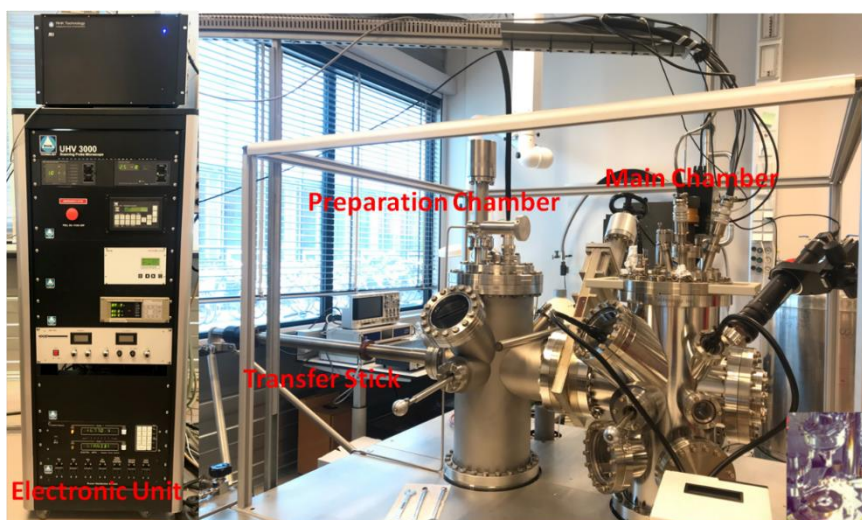
Figure 2.5. RHK STM system. Inset (right down corner): A scanner is place on top of the sample holder.

2.7. Experimental Methods

2.7.1. Au(111)

To obtain well-ordered SAMs an atomically flat and well-ordered substrate is a necessity (Ulman 1996). Usually a thin metal film (often gold) is deposited onto a glass, silicon or mica substrate. The metal films are grown by chemical vapour deposition of physical vapour deposition. The exact growth temperature and deposition rate determine whether an atomically flat film is obtained or not. The best results are usually obtained for a high growth temperature and a low growth or deposition rate.

In this study we have mainly used annealed Au films grown on a freshly cleaved mica substrate. It should be noted here that in the case of freshly cleaved mica substrates no adhesion layer (e.g. Cr or Pt) is needed (Colton 1998). The growth of Au on mica results into larger (111) oriented domains (Uosaki et al.,1995)

The bulk truncated Au(111) surface exhibits a simple hexagonal symmetry. A real Au(111) surface, however, reconstructs in the so-called herringbone structure. The herringbone reconstruction has a $22 \times \sqrt{3}$ unit cell. This cell that not contain, as one

would naively expect 44 atoms, but rather 46 atoms (Hanke and Björk 2013). The reason for the additional gold atoms is fact that the unreconstructed surface is under a tensile stress. By adding this extra atom this tensile surface stress can be relaxed resulting in a lowering of the surface free energy per unit area. The two bright rows, also referred to as soliton walls.
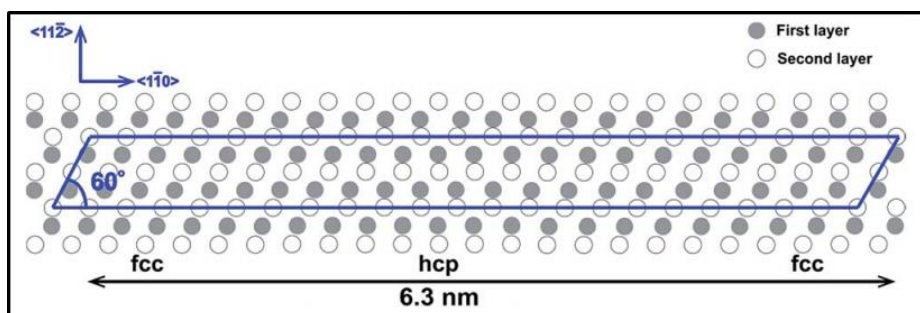
Figure 2.6. Schematic model of the herringbone reconstruction. Blue parallelogram indicates the $(22 \times \sqrt{3})$ unit cell. Reprinted (Source: Wu et al., 2015) with permission from The Royal Society of Chemistry.
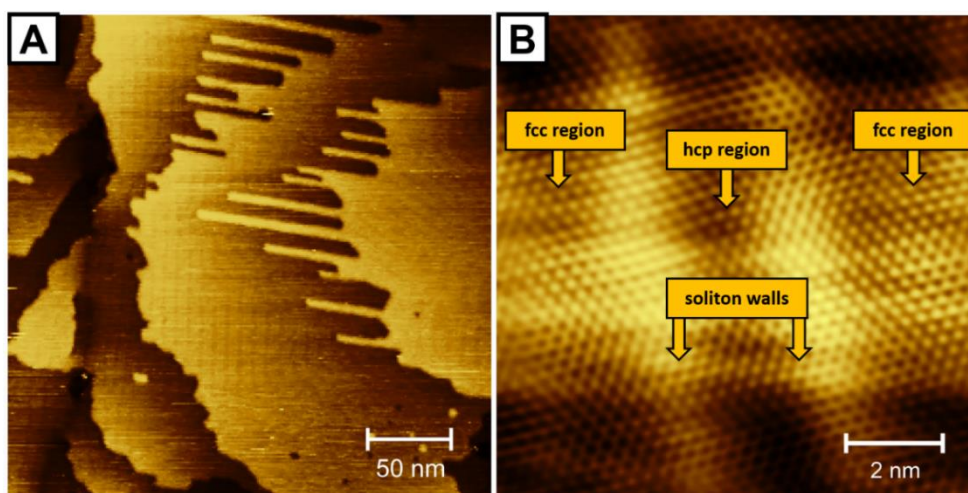
Figure 2.7. (A) STM images (290 nm × 290 nm) of the herringbone reconstructed Au(111) surface with gold 'fingers' recorded at a sample bias of 0.2 V and a setpoint current of 200 pA. (B) High resolution image of the herringbone reconstruction (10 nm × 10 nm). fcc and hcp regions are separated from each other by soliton walls.

Figure 2.6 and Figure 2.7(B) are caused by the fact that the surface atoms gradually shift from an fcc (face-centered cubic) position to a bridge position and then to

a hcp (hexagonal close packed) position. The periodicity of these soliton walls is 6.3 nm (Fitts et al., 2002). The periodicity of the soliton walls gradually increases when the reconstruction is lifted by the self-assembled molecules (Jewell et al., 2010).

In Figure 2.7 an STM image of the reconstructed clean Au(111) surface is shown. Two bright lines are visible in the image and the height differences between the fcc and hcp domains is 15 pm.

The Au(111) substrate is the most popular substrate of SAMs. The main advantages of using thin Au(111) films are (1) the material is inert and can therefore be used at ambient conditions (2) the thin films are easy to prepare and (3) of high quality. In addition the system can also easily be patterned by several lithographic techniques. Finally the system is also ideally suited for spectroscopic techniques such as, ellipsometry, surface plasmon resonance, quartz crystal microbalances and RAIRS (Love et al., 2005).
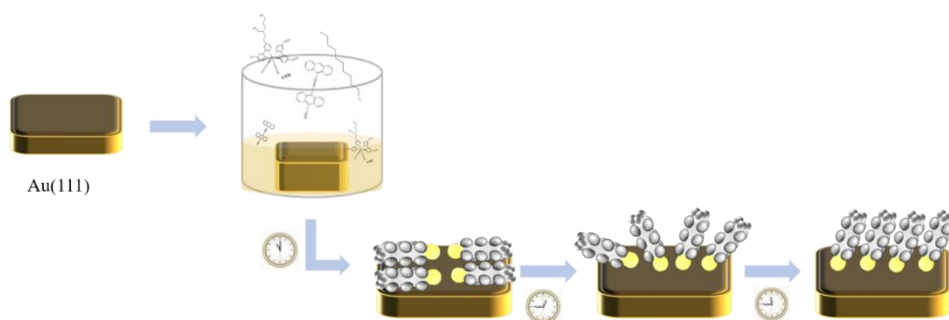
Figure 2.8. Schematic representation of the solution method for the preparation of self-assembled monolayers.

2.8. Sample Preparation

SAMs are formed by the adsorption of dissolved molecules in solution or growth from the vapor phase on a surface (Ulman 1996) . The most popular technique is solution deposition method. The quality of the SAM depends on the concentration of dissolved molecules, the exposure time, the temperature and flatness and cleanliness of the substrate (Noh and Hara 2000).

A freshly prepared clean Au(111) substrate is immersed into a solution of molecules (~ 0.005-10 mM), for 5-18 h at a room temperature (or slightly higher). The molecules in solution transfer from the liquid to solid substrate and form a well-ordered

monolayer. The quality of the SAM is optimized by tuning these parameters (Yang et al., 1995).

Densely packed and well-ordered SAMs can be obtained by using millimolar concentrations. It should be noted here that long immersion times usually improve the quality of the SAM since it helps to minimize the number density of defects (Love et al., 2005). Also, the solvent has a profound influence on the assembled morphology, binding sites, packing density and binding characteristics and helps to prepare defect-free ordered monolayer (Mamun and Hahn 2012). For that purpose a variety of solvents can be used, such as ethanol, N,N′-dimethylformamide (DMF), hexane, toluene, chloroform, etc. Mostly polar solvents are used for alkanethiol SAM preparation since non-polar solutions results in poor quality SAM that This is due to the interaction between the alkyl chains of the thiol monolayer and low-soluble molecules (Mamun and Hahn 2012).

It is essential to remove any contaminations from the surface before the substrate is immersed in the solution. Several techniques for substrate pre-treatments, such as piranha treatment, UV-ozone exposure (Ron et al., 1998), plasma cleaning, are applied. If a gold substrate is exposed to the ambient conditions, it is usually being extremely hydrophobic, which is a sign of organic contaminants (Nielsen and Lee 2013). These contaminants can be removed by for instance acidic piranha. Acidic piranha is a strongly oxidizing agent mixture of sulphuric acid (H_2SO_4) and concentrated hydrogen peroxide(H_2O_2) (30% (w/w) in H_2O) in 3:1(v/v) ratio. The films are immersed into the piranha solution for 30 minutes and then washed with copious amounts of pure water and dried with N_2 before using. Figure 2.8 shows the preparation of the SAM onto the substrate depending on the time.

2.9. Tip Preparation

The stability of the tip is of crucial importance when operating a STM since atomically resolved images can only be obtained by an ultra-sharp tip. The most frequently chosen material for STM tips that used for ultra-high vacuum experiments is tungsten (W). Ultra-sharp W tips can be prepared by electrochemical etching. The etching process is relatively simple; a tungsten wire is immersed in an electrolyte solution (for instance a 2 M KOH or NaOH solution). A tungsten wire serves as an electrode. A second electrode (a stainless wire ring-shaped wire) is positioned around the tungsten wire at the

air-electrolyte interface of the electrolyte. Subsequently the two electrodes are connected to an external power supply and a voltage (either DC or AC) is applied across both electrodes. At the cathode (the stainless-steel wire) and anode (the tungsten wire) the following reactions occur:

Cathode: $6H_2O + 6e^- \rightarrow 3H_2\ (g) + 6OH^-$

Anode: $\underline{W + 8OH^- \rightarrow\ WO_4^{2-} + 4H_2O + 6e^-}$

Overall: $W(s) + 2OH^- + 2H_2O\ \rightarrow WO_4^{2-} + 3H_2\ (g)$
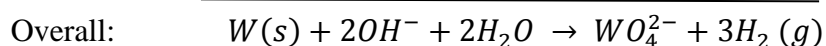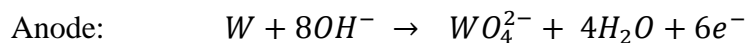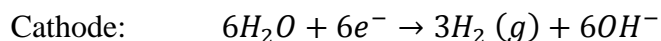
The meniscus at the tungsten tip should be well-defined and stable since it plays a crucial role in the formation of a sharp tip. An ultra-sharp apex of and small aspect ratio of the tip (tip length/shank diameter) are essential for stable and high-resolution STM measurements (Ju et al., 2011). The etching process is reproducible for a highly mechanical resistive material as W, however, W tends to oxidize and suffer from carbonaceous deposits (Rogers et al., 2000). The W-oxide can be removed in ultra-high vacuum by heating to about 800 °C (Setvín et al., 2012) or hydrogen plasma exposure (Vesel et al., 2010). An example of an electrochemically etched W tip is shown in Figure 2.9(B).

Alternatively, one can use a Pt/Ir STM tip made by mechanically cutting a wire or chemically etching. Pt/Ir tips are stable against oxidation and therefore these tips are preferred for ambient STM experiments. It has been shown (Gorbunov et al., 1993). Pt/Ir tips can be etched with a 1.5 M CaCl2 solution, resulting in a sharp tip apex and a low aspect ratio. In Figure 2.9A an example of an etched Pt/Ir tip is depicted. We have immersed the Pt/It wire into the solution by a depth of about 1-2 mm and subsequently applied a 40 DV voltages across the tip wire and the counter electrode.
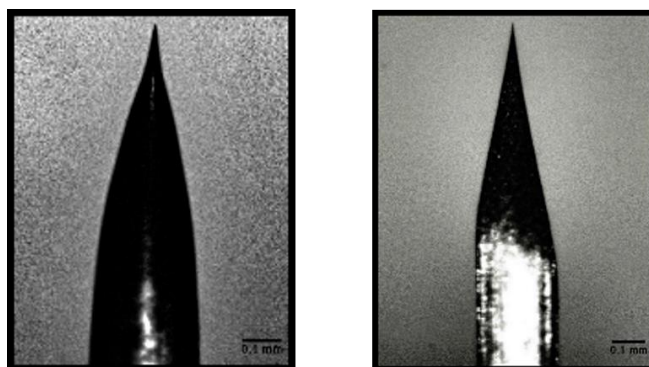
Figure 2.9. (A) Optical image of a 0.25 mm Pt/Ir electrochemical etched tip (5x zoom)
(B) Optical image of a 0.25 mm W electrochemical etched tip (5x zoom).

16

CHAPTER 3

STRUCTURAL DYNAMICS OF AIR-OXIDIZED DECANETHIOLS USING TIME-RESOLVED STM

3.1. Introduction

Surface modification of metal substrates via adsorption of organic molecules to form self-assembled monolayers (SAMs) has been extensively studied due to the easy fabrication of a uniform functional surface over a wide area (Ulman 1996, Love et al., 2005, Vericat et al., 2014). In order to integrate SAMs into functional devices, such as biosensors or molecular electronics (Chaki and Vijayamohanan 2002, Nerngchamnong et al., 2014), a fundamental and detailed understanding of the structural and electronic properties, dynamics and molecular interactions is required. The most popular model systems for self-assembly are alkanethiols on Au(111) substrates because of their convenient preparation by chemisorption from dilute solutions. (Vericat et al., 2010). Often unfunctionalized alkanethiol SAMs are used as an insulator or as a host for inserted conjugated molecules. However, the stability of alkanethiols on Au(111) is one of the most important issues for their applications in ambient environments in which long-term use is required (Srisombat et al., 2011). In addition, the alkanethiol SAMs provide well-defined structures with predictable interfacial properties (Poirier 1999, Qian et al., 2003).

There have been numerous studies regarding the structure of alkanethiol SAMs on Au substrates. The structure of the SAMs depends on the chain length, surface coverage, temperature and substrate morphology (Poirier 1999, Sotthewes et al., 2013). Using scanning tunneling microscopy, in total over ten different phases are observed, with the most common the centered $(23 \times \sqrt{3})$ phase (β), the hexagonal $(5\sqrt{3}x\sqrt{3})R30°$ phase (δ) and the centered $(3 \times 2\sqrt{3})$ standing up phase (ϕ), which is found at full coverage. In real-space images of decanethiol self-assembled monolayers one often finds a coexistence of several phases, mixed phases, anti-phase boundaries, vacancy islands and ad-islands (Toerker et al., 2000, Poirier et al., 2001). Besides, the decanethiol SAMs show phase transitions and dynamic behaviour revealing that these SAMs are structural not fully stable (Wu et al., 2013).

When exposed to air, the gold-thiolate bond degrades into alkanesulfonates with ozone as the main precursor for the oxidation (Schoenfisch and Pemberton 1998, Poirier et al., 1999). The rate of oxidation depends on the morphology of the surface, the concentration of oxidants (e.g., ozone) in the ambient atmosphere and the alkyl chain length (Hutt and Leggett 1996, Cortés et al., 2009). Tarlov and Newman discovered, using static secondary ion mass spectrometry, that alkanethiolates SAMs exposed to ambient environment experience oxidation of the sulfur headgroup (Tarlov and Newman 1992). On the contrary, such sulfonate species were not found in SAMs after long term storage in UHV (ultra-high vacuum) the absence of light (Noh et al., 2006). Further spectroscopy studies found the alkanethiolate SAMs on gold can be easily oxidized to alkanesulfinates and alkanesulfides after exposure to ambient conditions (Burroughs and Hanley 1993). These compounds are not chemisorbed but instead weakly bonded to the surface leading to a deterioration of the alkanethiolate SAM (Willey et al., 2005). Other studies suggest scissoring of the S-C bond due to oxidation leading to desorption of alkyl chain fragments and oxidation of the surface-bound sulfur (Lewis et al., 1995, Hutt, et al., 1998). Sotthewes et al., have showed that decanethiol SAMs oxidize when the monolayer contacts with the air and transforms into decanesulfonates (Sotthewes et al., 2018). The decanesulfonates arrange in a lamellae-like structure (λ phase) without affecting the herringbone reconstruction of the Au(111) surface indicating that the interaction between the molecules and the surface is rather weak. Both decanethiols and decanesulfonate phases co-exist on the surface and do not intermix.

Different adsorption configurations do not only affect the interfacial properties of surface, also the dynamic properties. Even after a molecule is adsorbed onto a substrate, it can still exhibit dynamic behaviour (Stipe et al., 1997, Schaffert et al., 2013). Current-time spectroscopy (I(t)) makes it possible to study these dynamic processes down to the level of a single molecule (Sotthewes et al., 2015, Wu et al., 2013). The dynamic behaviour of the SAM is unique for its configuration giving indirect evidence for the structural ordering within the SAM. Here we investigate the structural stability of the decanethiol and air-oxidized decanethiol (decanesulfonates) SAMs by space- and time-resolved scanning tunneling microscopy. We show that the decanesulfonate phase shows less dynamic behaviour and is structural more stable compared to the decanethiol phases. A two-dimensional activity map reveals that all the dynamics within the decanesulfonate phase are observed within the vacancy lines. The switching process is

stochastic and is caused due to the small displacement of the sulfonate part of the molecule.

3.2. Experimental

3.2.1. Scanning Tunneling Microscopy

All the STM measurements were conducted with an UHV STM (see Figure 2.5, RHK Technology UHV3000) at room temperature with a pressure 1×10^{-10} mbar. STM tips prepared from tungsten wire with electrochemical etching process.

3.2.2. Contact Angles

Microliter droplets are created by employing a computer-controlled syringe (OCA15+ goniometer, Dataphysics, Germany); the droplet volume is equivalent to 0.5 µl and is accurate to within 5%. The measurements of the contact angle at the solid-liquid-gas interface were performed immediately after substrate functionalization and drying. The contact angles during the preparation process are given in Table 3.2.

3.2.3. Sample Preparation

Decanethiol (purity 99%) was purchased from Sigma-Aldrich (Steinheim, Germany) and used without further purification. ($11 \times 11\ mm^2$, 250 nm Au on 2 nm Cr on borosilicate glass) for STM measurements were purchased from Arrandee (Werther, Germany). Au(111) samples were obtained by annealing these substrates in a high purity H_2 flame for 5 min. Decanethiol SAMs were obtained at room temperature by chemisorption from a 1 mM ethanolic solution onto freshly prepared Au(111) substrates for 24 h. It is common knowledge that this immersion step leads to a densely packed SAM where the decanethiolate molecules form a standing up phase. In order to reduce the coverage, we immersed our sample in a pure ethanol solution for 1 h. After thorough rinsing of the decanethiol SAMs with pure spectroscopy grade ethanol, the samples were loaded into UHV STM for imaging. To pre-check the presence of the SAMs on the

Au(111) surface, contact angle measurements were carried out. The values of the advancing and receding contact angles were 92° and 80° , respectively. This result is in agreement with the observations of Li et al., (Li et al., 2006). STM topography for the freshly annealed Au surface showed the herringbone reconstruction characteristic of clean Au(111).

3.3. Results and Discussion

STM image of an air-oxidized decanethiol self-assembled monolayer on Au(111) is shown after two weeks of exposure to ambient conditions in Figure 3.1. Three distinctive phases are present on the surface, the β phase, a fluid-like phase and the λ phase. The β phase is a centered $(23 \times \sqrt{3})$ striped phase where the decanethiols lie flat down on the surface in an alternating head-to-head and tail-to-tail registry. The inter-stripe distance is approximately 3.3 nm and with a 0.49 ($\sqrt{3}$ times the Au(111) lattice constant (2.884 Å)) periodicity along the stripes. The stripes in the β phase can shift perpendicular to the row direction by roughly half of the row spacing (see Figure 3.1(A)). In contrast to the surface prior to oxidation, the terraces are no longer completely covered with decanethiol phases.

The β phase is still present on the surface, whereas the δ phase has disappeared. Instead a significant fraction of the near-surface region converted into a fluid-like phase. The fluid-like phase has no periodic order and the molecules diffuse around the surface (Poirier et al., 1999, Wu et al., 2013). This is in good agreement with the observed changes in the XPS data which is on the literature (Sotthewes et al., 2018).

Survey XPS spectra of decanethiol SAMs that are freshly prepared or stored for 2 weeks in ambient conditions are shown in Figure 3.2. The spectra of the Au 4f region shows that exposure to ambient conditions results in no decrease of Au photoemission and no detectable broadening (see Figure 3.3).

Table 3.1 summarizes the S 2p peak area compared to the Au 4f peak area for both the oxidized and the non-oxidized SAM.

The thiolate peak (162 eV) represents the sulfur atoms which are bound to the Au surface. The sulfonate (168 eV) peak represents the sulfur atoms which reacted with oxygen. No sulfonate signal was found for the SAM before oxidation as there is no oxygen available to react with. For the oxidized sample the ratio between the thiolate and

sulfonate is approximately 50%. The estimated coverage of the λ phase is approximately 45% (based on roughly 40 images).
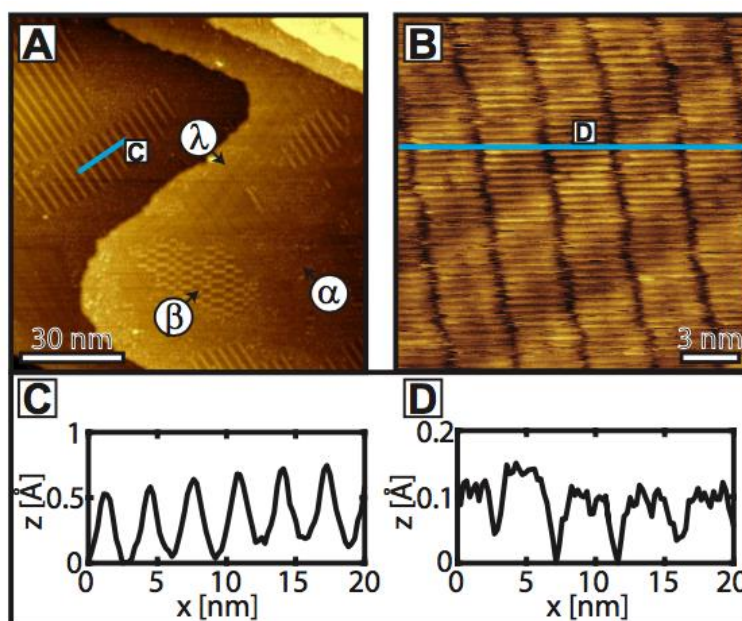
Figure 3.1   (A) STM topography image (100×100 nm^2) of decanethiol SAM on Au(111) after 2 weeks of exposure to ambient conditions. The tunneling parameters are 190 pA and 1.20 V. (B) Zoomed image (20×20 nm^2) of the λ phase. The herringbone reconstruction of the Au(111) surface is preserved indicating a weak interaction between the molecules and the surface. Tunneling current 55 pA, sample bias 200 mV. (C) Cross-sectional height profile from corresponding line segment in (A) (D) Cross-sectional height profile from corresponding line segment in (B) revealing a 3.5 nm width of the fine-striped domains.

A decrease in the intensity of the C 1s peak is observed which is attributed to the desorption of molecules during oxidation. Desorption leads to a lower surface coverage, and thus to phases with a lower density. Therefore, the high-density phase disappears after oxidation and the low-density fluid phase arises. The cross-sectional height profile in Figure 3.1 shows that the inter-stripe spacing in the phase remains approximately 33 Å. In addition to the two decanethiol phases, another stripe-like phase is present on the surface.

Figure 3.1(B) shows a zoomed image of the λ phase. The λ phase is composed of fine-striped domains with a width of approximately 3.5 nm separated by vacancy lines which run perpendicular to the fine stripes (see Figure 3.1(D)). The stripes are aligned along one of the closed packed directions of the Au(111) substrate (<01**1**>). The fine-

stripe direction makes an angle of 30° with the ridges of the herringbone reconstruction (which run in <11**2**> directions). The separation between the fine stripes is √3a, i.e. 0.5 nm. The fine stripes of neighbouring domains are always out-of-phase. Since the λ phase is only observed after exposure to air, we assume that the molecules in the λ phase are oxidized. In addition, previous studies on decanethiol SAMs characterized all of the structural phases for decanethiols on Au(111) including phases due to annealing or oxidation (Qian et al., 2003, Fitts et al., 2002). None of the observed phases matches the characteristics of the λ phase. Poirier et al., investigated the oxidation process using STM. However, they were unable to find a structured phase of oxidized decanethiols. The oxidation procedure was different compared to the procedure followed in this study. Instead of using air, they performed their experiments in an ozone environment. This probably results into a lower density of oxidized molecules on the surface and thus to a disordered rather than an ordered phase.
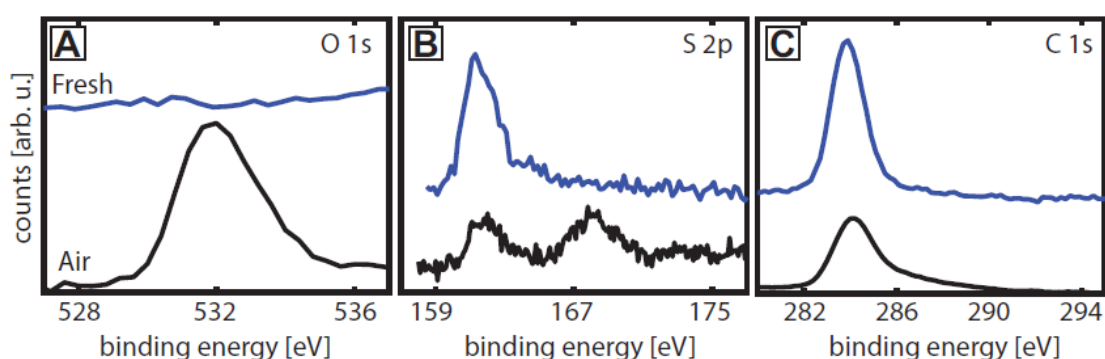
Figure 3.2. XPS spectra obtained from decanethiol SAMs on Au(111). Spectra in blue are from a fresh sample while spectra in black are from a sample exposed for 2 weeks to ambient conditions. (A) Spectra of the O 1s region showing that the monolayer exposed to air contains oxygen in contrast to the fresh sample. (B) Spectra of the S 2p region showing a reduced intensity of the S−Au bond peak in the air-exposed sample. A second peak appears corresponding to oxidized S species. (C) Spectra of the C 1s region showing that the monolayer exposed to air exhibits loss of carbon intensity.

The fact that the herringbone reconstruction is visible and unaffected by the SAM implies a weak interaction between the Au(111) surface and the molecules (Rossel et al., 2008, Jewell et al., 2012). The herringbone reconstruction contains 23 atoms in the top layer placed on 22 atoms on the second layer resulting in a (22 × √3) unit cell (Wöll et al., 1989). Both fcc and hcp domains are included in an alternating order leading to a

slightly elevated ridge of about 15 pm. When molecules interact with the herringbone reconstructed surface, both the fcc/hcp ratio and the unit cell become larger till the reconstruction is completely lifted (Jewell et al., 2012, Rossel et al., 2008). For the λ phase both of the effects are not observed, indicating a rather weak interaction between the molecules and the Au(111) surface. The height variation within the λ phase is much smaller compared to the β phase (see Figure 3.1(C)-(D)). In a previous study, it is explained this difference due to the mixing of the sulfur orbitals. In the β phase the orbitals of the sulfur atoms and the gold surface mix leading to a bright appearance in the STM images (Zeng et al., 2002). When sulfur atoms react with oxygen atoms, as is the case in the λ phase, no mixing of orbitals occurs and therefore smaller height differences are measured.
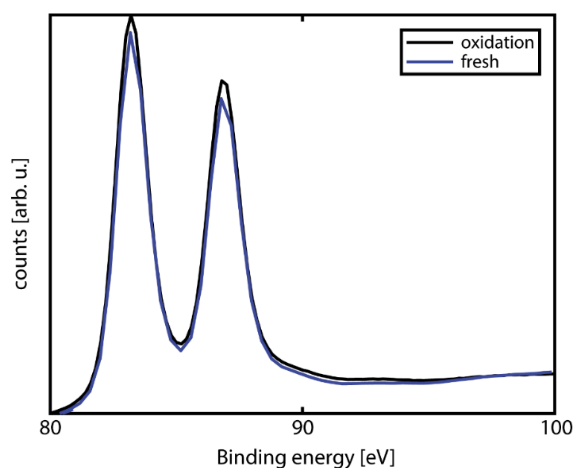
Figure 3.3. XPS spectra of the Au 4f region obtained from decanethiol SAMs on Au(111). Spectra in blue are from a fresh sample while spectra in black are from a sample exposed for 2 weeks to ambient conditions.

In Figure 3.4 an STM image of a freshly prepared decanethiol SAM on Au(111) is shown. Both the β and δ phase are present on the surface, which co-exist on the surface in agreement with previous studies (Qian et al., 2003, Wu et al., 2013). Besides these phases, also several characteristic defects, such as substrate steps, ad-islands and vacancy islands are present on the surface together with a fluid-like phase. The depth of the vacancy island (see Figure 3.4(A)) is one atomic Au layer and thus a vacancy in the Au(111) substrate and not a defect in the SAM. Additional evidence in favour of this observation is found within the vacancy, where an ordered decanethiol monolayer is found.

Table 3.1. Ratio of the XPS S 2p thiolate and sulfonate peaks with respect to the Au 4f before and after oxidation

Sample	S 2p area/ Au 4f area	
	thiolate	sulfonate
SAM before oxidation	0.0414	-
SAM after oxidation	0.0274	0.0296

The dynamic behaviour of the SAM is unique for its configuration giving indirect evidence for the ordering within the SAM. In order to probe the dynamic behaviour of the different phases, current-time (denoted as I(t)) spectroscopy is performed. Figure 3.4(B) and Figure 3.4(C) show I(t) traces performed on the β phase and the fluid-like phase, respectively. The set points were set at 200 pA and 1.2 V. The I(t) spectroscopy performed on the fluid-like phase (see Figure 3.4(C)) exhibits a rich dynamical behaviour and extremely high current values. The current profile is explained due to molecules diffusing rapidly underneath the tip apex. When the alkyl tail of the molecule flips up and contacts the tip, the current increases rapidly due to the different tunneling path (Kockmann, Poelsema, and Zandvliet 2009, Sotthewes et al., 2014). This observation is in favour of the the RS-Au and/or RS-Au-SR complexes (Maksymovych et al., 2006, Gao et al., 2016). In order to measure dynamics in the decanethiol SAM, i.e. movement of the decanethiols, the strong covalent S-Au bond needs to be broken, which is very unlikely. When a complex is formed, the interaction between the gold surface and the complex is much weaker as compared to that to the Au-S bond (Grönbeck and Odelius 2010, Häkkinen 2012), and therefore the diffusion energy is substantially lower explaining the observed behaviour.

The I(t) trace of the β phase performed on the bright part, i.e. the sulfur atom, reveals a two-level switching process (see Figure 3.4(B)). The origin of the fluctuations in the current can be attributed to several dynamic processes, such as diffusion of the molecules or wagging of the alkyl tails. In the case of wagging of the alkyl tail, larger current fluctuations are expected. Also, in the case of diffusion in which a molecule moves outside the probed surface, larger current fluctuations have been observed. Changes in the molecular configuration is another mechanism where current fluctuations are reported. The molecule does not diffuse away from the tip, but simply another part of

the molecule is probed. As shown in a previous study (Wu et al., 2013), the decanethiol is very mobile and therefore it is very likely that the decanethiol SAM is diffusing as a blanket underneath the tip. Thus, the variation in the tunneling current could be attributed to the contribution from different parts of the decanethiol molecule, i.e. from the sulfur alkyl tail.
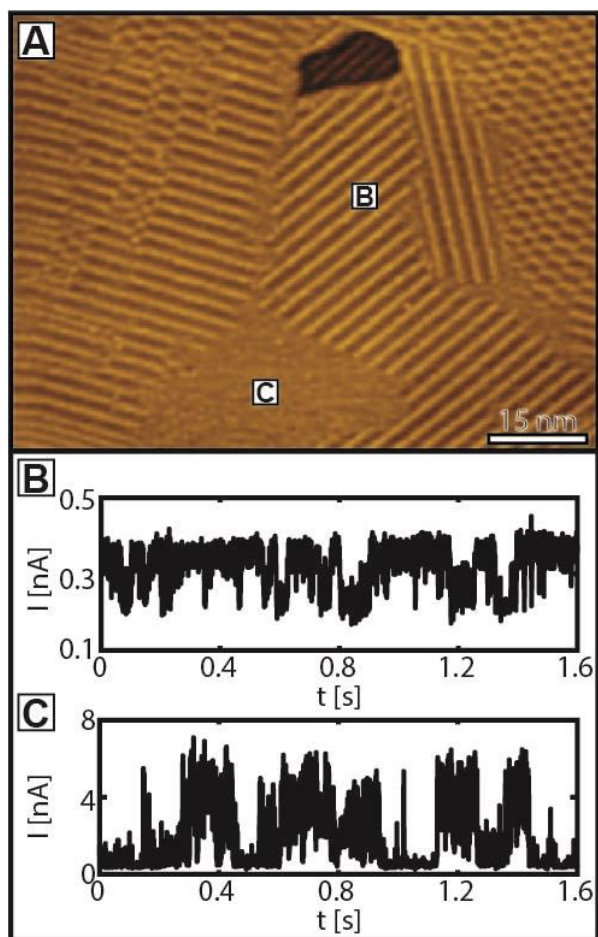
Figure 3.4. (A) STM topography image ($100 \times 75nm^2$) of a decanethiol SAM on Au(111) showing the various phases at room temperature. Most of the terraces are covered with the β or δ phase. Occasionally a fluid-like phase is present on the surface. The tunneling parameters are 190 pA and 1.20 V. (B) I(t) spectroscopy performed the bright stripe of the β phase and (C) on the fluid-like phase. The set point values are 200 pA and 1.2 V. The I(t) traces on the β phase show a two-level switching process, while the I(t) spectra of the fluid-like phase exhibits a rich dynamic behaviour.

The I(t) spectroscopy can be considered as a fingerprint for the different decanethiol phases found on Au(111). Therefore, I(t) spectroscopy can give indirect evidence for the structural properties of the SAM.
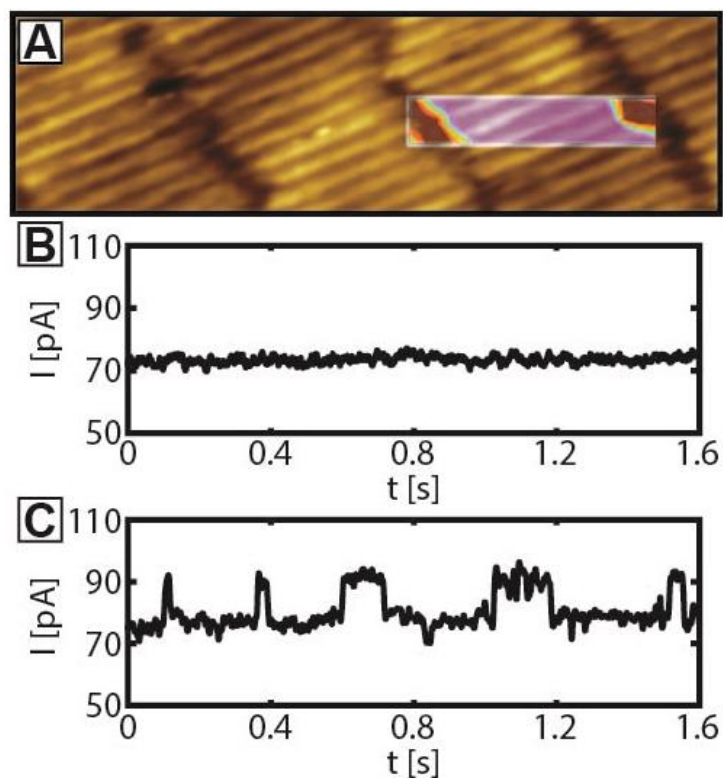
Figure 3.5. (A). STM topography image (15×5 nm^2) with a two-dimensional activity map of the amount of activity as a function of position for 120 individual I(t) traces. The color spectrum scales from dynamic (red), many current fluctuations, to static (blue), constant current. (B) An exemplary I(t) trace recorded on the molecular stripes (blue area of the activity map). (C) Characteristic I(t) trace recorded on the vacancy lines between the molecule stripes (red area of the activity map). The set points are 75 pA and 200 mV.

In Figure 3.5(A) an STM image of an air-oxidized decanethiol SAM on Au(111) is shown. Within the image, a spatially resolved activity map of 120 individual I(t) traces is presented. The colour map is a measure of the number of current switches per time interval, red stands for a large number of current switches, whereas blue stands for a small number of current switches. When the tip is positioned at the middle of the fine stripes (blue area) only occasionally current fluctuations are observed (Figure 3.5(B) shows a characteristic I(t) trace on top of a stripe (blue area)). Probably, intermolecular and molecule-substrate van der Waals forces prevent the alkyl chains to alter within the monolayer. When the tip is located in the vacancy line (red area), the current flips back and forth between two well-defined levels (Figure 3.4(C) shows a characteristic I(t) trace taken at a vacancy line (red area)).
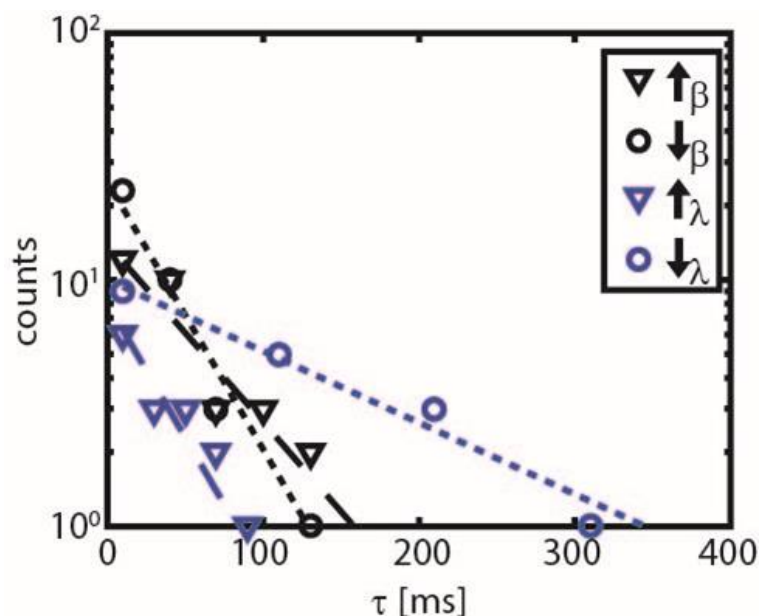
Figure 3.6. A semi-log plot of the residence time (τ) of the "up" (↑) and "down" (↓) states of the β and λ phase. A clear preference for the "down" configuration is found for the λ phase. The dashed lines are theoretical fits for a stochastic process (Poisson distribution).

The I(t) spectroscopy traces on both the sulfur atoms of β phase and the oxidized sulfur group of the λ phase exhibits a two-level switching process. However, the frequency of switching is in the β phase much higher compared to the λ phase. For the β and λ phase, a switching frequency of approximately 30 Hz and 15 Hz is found, respectively. When the counts distribution of residence time (τ) is plotted on a semi-logarithmic scale in Figure 3.6, both systems exhibit a linear dependence, characteristic for a stochastic, i.e. random, process. From the slope of the curves, the average residence time ($<\tau>$) can be extracted. For the β phase the residence times for the "up" and " down" states are equal to approximately 50 ms, whereas in the case of the λ phase a clear preference for the "down" configuration is found (the residence times of the "up" and "down" states are approximately 40 and 150 ms, respectively). Although in both cases a stochastic process is on the basis of the dynamic behaviour, there is no state preference in the β phase whereas there is a clear preference in the λ phase. In the β phase the dynamic behaviour is caused by the movement of the complete phase over the surface. Every time another part of the molecule is probed leading to current fluctuations. In the λ phase the molecules are static, i.e. no movement is observed within the SAM, and the current fluctuations are most probably caused by a hindered translation, rearranging the oxidized

sulfur group. Clearly there is a preference for the lower state where the oxidized sulfur group is lying on the surface while the "up" state is. The clear preference in the λ phase also explains the difference in switching frequency. In order to approve the existence of the decanethiol monolayer, current-voltage (I-V) spectroscopy was carried out on the surface by the standard method of switching off the STM feedback loop during the time of the bias voltage sweep. A representative current–voltage spectrum of on the decanesulfonates (oxidized decanethiol) molecules SAM on Au(111) is shown in Fig. 5 and revealed a semiconducting current-voltage, i.e. I(V), signature (see Figure 3.7).
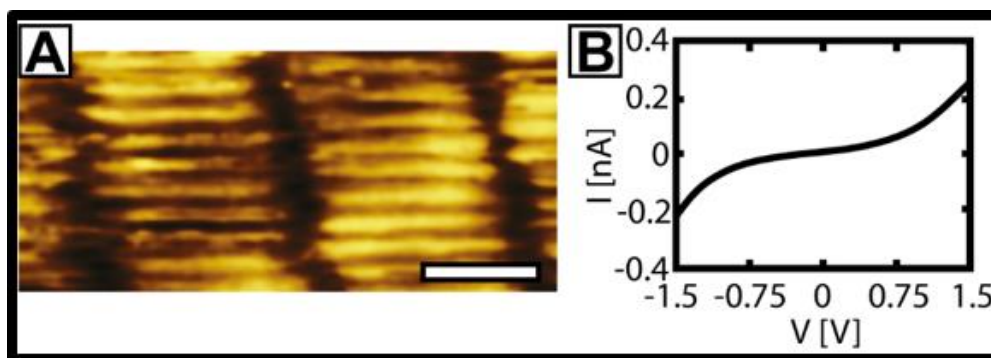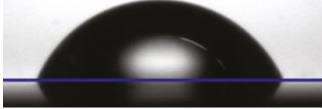
Figure 3.7. (A) Zoomed topography image (10×10 nm^2) of the decanesulfonate (λ) phase. Tunneling current 55 pA, sample bias 200 mV, scale bar is 2 nm. (B) Current-voltage (I(V)) curves recorded on the λ phase in.

When a freshly prepared Au(111) substrate was immersed in a 1mM ethanolic solution for 24 h, the contact angle was equal to $104\pm2^{\circ}$ in good agreement with previous studies. In order to reduce the coverage, the sample was immersed in a pure ethanol solution for 1h. The contact angle dropped to about 90°, as expected for a low coverage sample. When the sample was exposed to air for 2 weeks, the contact angle slightly decreased, owing to a fraction of the molecules that desorb during the oxidation process (Poirier et al., 1999, Schoenfisch and Pemberton 1998).

Although ease of preparation and stability of alkanethiols SAMs on gold are thus far unmatched by any other system for SAM formation, the often made assumption that the gold− sulfur bond is ultrarobust and stable under ambient conditions is false. The instability of the decanethiol monolayer at room temperature and the process of oxidation at ambient conditions have a massive impact on the structure of the monolayer, which is highly undesirable for ambient condition electronics. However, the oxidized decanethiol

(decanesulfonates) molecules form a new phase which shows no structural fluctuations within the monolayer.

Table 3.2.   Contact angle at different stages of the preparation procedure

	measured CA(°)	expected CA(°)	
Bare gold	60±2	66 (Smith 1980, Kutsenko et al., 2017)	
Freshly prepared sample	104±2	105 (Li et al., 2006)	
After immersion in pure ethanol	89±2	85 (Li et al., 2006)	
After oxidation for 2 weeks	87±2		

3.4. Conclusion

In conclusion, the dynamic behaviour of decanethiol and air-oxidized decanethiol SAMs on Au(111) has been investigated using current-time scanning tunneling spectroscopy. For the air-oxidized decanethiol SAM a two-dimensional activity map of individual current-time traces reveals that all the dynamics take place within the vacancy lines. A stochastic two- level switching process is found, however, with a clear preference for one configuration. The I(t) traces provide additional evidence for the proposed models of the various phases and should be considered as fingerprints for the

different decanethiol and air-oxidized decanethiol phases found on Au(111). The herringbone reconstruction of the Au(111) remains intact, and the SAM structures are remarkably stable at ambient conditions.

CHAPTER 4

OXIDATION OF ANTHRACENE BASED ALKYNE LIGAND MOLECULE ON AU(111)

4.1. Introduction

Self-assembled monolayers (SAMs) can be used in numerous advanced applications ranging from molecular electronics (Love et al., 2005), controlled wetting (Abbott et al., 1995), corrosion inhibition (Jennings and Laibinis 1996), protein absorption (Harder et al., 1998), lubrication (Bliznyuk et al., 1998), adhesion (Kessel and Granick 1991) to biosensors (Franks et al., 2007) . Each application requires different physical properties of the SAM, which can be realized by selecting the proper molecule-substrate combination. The binding of the molecule occurs in the vast majority of cases on a metal surface, such as gold, copper, silver, palladium or mercury, via a specific terminal group of the molecules (Love et al., 2005). The electronic properties of the SAMs are controlled by the binding of the molecule to the substrate, the substrate and, of course, the molecule itself. As binding groups of the SAM molecules the following groups have been used: pyridines (Finklea and Hanshew 1992), nitriles (Steiner et al., 1992), isocyanides (Lin and McCarley 1999), disulfides (Palegrosdemange et al., 1991), carboxyclic acids (Folkers et al., 1995), phosphines (Jewell et al., 2010) and thiols. So far, most commonly studied SAM is the thiol bonding gold substrate system (R-S-Au) (Tour 2003). The main problem of the thiol based SAMs is the oxidation and photoinduced effect which leads to multilayer formation (Crudden et al., 2014). Sotthewes et al., showed that decanethiol molecules oxidize at ambient conditions and have a huge impact on the structural instability of the monolayer, which is highly undesirable for ambient condition applications. The oxidized decanethiol (decanesulfonates) molecules form a new phase that does not show any structural fluctuations within the monolayer. However, this new phase does not have a chemical bonding to the substrate, the molecules are only physisorbed onto the Au(111) substrate. . One of the main aims of the SAM community is to search for very stable and efficient SAM molecule-substrate systems that can be used for technological applications. Alkyne

binding molecules are a suitable candidate compared to the thiol groups with regard to the quality of the SAM, sensitivity to oxidation, chemical and thermal stability and transport properties (conductivity) (Pla-Vilanova et al., 2015, Sun et al., 2014, Bejarano et al., 2018, Kang et al., 2012).

Oxidation is the main problem during the formation of the SAM also for the alkyne end group molecules when bound to the gold substrate at the ambient conditions (Zaba et al., 2014, McDonagh et al., 2007). O_2 free atmosphere prevented the alkynes from oxidation during the formation of the SAM (Zaba et al., 2014). For alkyne binding molecules several structures are proposed in the literature; upright and flat-lying configurations, on atop, bridge and hollow sites, by dehydrogenation or oxygenation on gold surfaces. Computational studies have shown that the most favourable alkyne binding occurs between carbon and the Au(111) substrate. The covalent bond is formed by removing the terminal hydrogen from carbon, which results in an upright position on the fcc lattice site (Zhang er al., 2007, Tang and Jiang 2014, Maity et al., 2013).

Synthesized anthracene-based molecules have an alkyne end group which are referred to as 9-(anthracen-9-ylethynyl)-10-ethynylanthracene (EAEA) molecules. We have designed the molecule and have taken into account several properties to enlighten the alkyne binding properties to the Au(111) substrate and the effect of the large- π systems on the formation of ordered structures. The molecules, which exhibit a delocalized π- symmetry, are used as molecular wires in molecular electronic applications (Emberly and Kirczenow 1998) and anthracene based organic molecules are used in organic electronics, optoelectronics and photochemistry due to their aromatic structure and photo reactivity (Shi 2013). In terms of applications, well-designed EAEA molecules have profound advantages such as switching of the molecule induced by UV light wavelength accompanying by a dimerization process (Fox and Wooten 1997). Additionally, the acetylene axis (spacer alkyne) conduces to long-range ordering in SAM formation (Dhirani et al., 1996) and allows the rotation between two anthryl groups, which is used in molecular rotors, sensors and switches (Toyota et al., 2010).

Up to now, there have only been a few studies which have investigated the formation of self-assembly monolayers on the Au(111) surface with the alkynyl end group molecules. The exact details of the binding motif and affinity of the SAM structure alkyne end group molecules are still not completed known.

Self-assembled monolayers on Au(111) surfaces are studied and optimized by various experimental techniques including scanning tunnelling microscopy (STM), X-

Ray photoelectron spectroscopy (XPS), Polarization-Modulation Infrared reflection-absorption spectroscopy (PM-IRRAS), water contact angle (CA) measurements. The obtained results allows us to understand the binding properties of the alkyne groups to the Au(111) surface. We conclude that the alkyne oxidation occurs at ambient conditions, but the ordered structure still exhibit chemical bonding between the carbon atoms of the molecule and the gold atoms of the substrate. These results are significantly different from the oxidized thiol molecules on Au(111), which only exhibit a physisorbed interaction with the substrate. Based on these results it is clear that alkyne SAM systems are very interesting candidates for ambient molecular electronics applications.

4.2. Materials

Au(111) was purchased commercially from Phasis, Switzerland. The typical gold thickness is 150 nm. Chemicals were used without further purification: Ethanol (>99%, Aldrich), 2- propanol (Merck , for analysis), H_2O_2 (Aldrich 34,5-36,5%), H_2SO_4 (95-97%, Aldrich), pure water (Merck Millipore), KOH (>99.97, Sigma-Aldrich). The structure of the synthesized molecules was checked by using ^{12}C (100 MHz) and ^1H (400 MHz) NMR methods.

4.3. Au(111) Surface Cleaning and SAM Deposition

The synthesized 9-(anthracen-9-ylethynyl)-10-ethynylanthracene (EAEA) molecule is shown in Figure 4.1. The synthesising methods were conducted with Pd/Cu catalysed Sonogashira with the very much appreciated support from our colleague Muhammed Üçüncü.

EAEA-SAMs were prepared by immersing the Au(111) substrate into 5 μM ethanolic solution. The glass tube was sealed and kept 16 h at 60 ^{o}C. All glassware was immersed in a fresh acidic piranha solution (H_2O_2/H_2SO_4, 3:7, v/v) sequentially and basic piranha solution (H_2O_2/KOH/2-propanol, 15:15:1, v/v) and rinsed several times with ultrapure Milli-Q water before usage. The Au(111) substrate was removed from the

solution and rinsed with copious amounts of solvent and dried by N_2 gas. These treatments remove surface contaminants and atmospheric carbon.
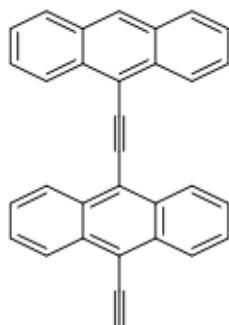
Figure 4.1.   Structural Formula of EAEA molecule

4.4. SAM Characterization

STM imaging was conducted using a Nanosurf Easy Scan 2 system at ambient conditions and at room temperature. Imaging was performed in the constant current mode using tunnelling currents between 200 and 250 pA and bias voltages between 0.2 and 0.5 V. The piezo scanner of the STM was calibrated by measuring the surface lattice constant and atomic step height of a freshly cleaved graphite surface. The analysis of the images were performed by using the scanning probe microscopy data analysis software Gwyddion.

Scanning tunnelling spectroscopy measurements were also conducted with the Nanosurf Easy Scan 2 STM. During the I/V measurements the feedback loop was deactivated and ramping of the voltage was performed at a constant tip-sample distance. The reproducibility of I/V spectra are checked by recording and analysing both forward and backward sweeps with different tips for multiple times.

A Woollam spectroscopic ellipsometer M-2000X was used to measure the thickness of the SAM layer with has a spot size of about 2 mm. The data has been fitted with a Cauchy layer model. The wavelength range is from 245 nm to 1000 nm and we used a fixed incidence angle of 65.82°.

XPS data were recorded with a PHI Quentera SXM photoelectron spectrometer. Al Kα-radiation was used to obtain the XP spectra of the SAMs with a 200 μm spot size.

The spectra were recorded at constant analyser energy (CAE) mode with analyser path energies of 150 eV for the survey spectra and 1000 eV for high-resolution spectra.

PM-IRRAS experiments were conducted and recorded with a Thermo Scientific Nicolet. The Table-top Optical Module with 4 cm^{-1} resolution in the reflection mode typically collects 2000 scans. The reflection absorption was measured at 80° angle to obtain high intensity.

4.5. Results and Discussions

Self-assembled monolayers of EAEA molecules on Au(111) substrates were prepared in order to investigate the binding properties and the motif of the SAM. The SAM formation was optimized by varying the temperature, concentration and immersion time of the immersion process. The SAM preparation was carried out under ambient conditions at 60 °C. Monolayers were characterized by water contact angle (CA) measurements to check the film formation of a freshly prepared synthesized EAEA molecule on Au(111) as well as the bare Au(111) surface. A contact angle of 80° was found for the EAEA treated sample, while an angle of 62° was found for the bare gold substrate under the same experimental conditions with an accuracy of ±1°. The water contact angles of closed-packed single crystal anthracene were found to be 94°-95°, which is in agreement with our result (Fox, Hare, and Zisman 1953). Ellipsometry was used for the determination of the thickness of EAEA covered Au(111) surface, yielding a thickness of 0.9 nm±0.1 nm for the self-assembled monolayer. This value is very close to 1 nm, which is the theoretically predicted molecular length of the EAEA molecule The very small deviation in thickness (0.9 nm versus 1 nm) is most probably related to the presence of some low density domains. The latter is confirmed by the numerous STM images that we recorded.

The monolayer structures of the EAEA molecules on the Au(111) substrate was obtained by solution deposition method at ambient conditions. Alkyne molecules are oxidized at ambient conditions during the SAM deposition process (Zaba et al., 2014). Different oxidation products, such as carboxylic acid, epoxide (McDonagh et al., 2007), glyoxalic acid and oxalic acid (Hay 1965) can be formed during the oxidation process. XPS spectra were recorded to confirm the adsorption of the molecules on Au(111) and to determine the possible oxygenated groups of the EAEA molecules. The representative

XPS data are displayed in Figure 4.2. All spectra were recorded with respect to known reference binding energy of gold Au 4f7/2. XPS peaks at 84.46 eV and 88.13 eV are observed in Figure 4.2(A). These peaks are characteristic for non-oxidized gold peaks. Figure 4.2(B) shows a C 1s spectrum. Polar ethanol solvent had been used for the SAM preparation. The peak at 284.78 eV is a characteristic for a carbon atom in an aromatic ring with sp^2 hybridization. The C=C feature is characteristic for the anthracene groups of the molecule (Diaz et al., 1996). The binding peak related to the interaction between the metal and carbon is located below the 283 eV, as predicted by DFT calculations. The typical binding energy of methylacetylide is located at 283.7 eV on Au(111. This C-Au bonding shows up as a low-energy shoulder in the main peak. However, the dominant feature of the C 1s aromatic peak dominates at low binding energy and therefore the protrusion around 283 eV cannot be resolved in the spectrum. (Zhang et al., 2012, Sohn et al., 2007).
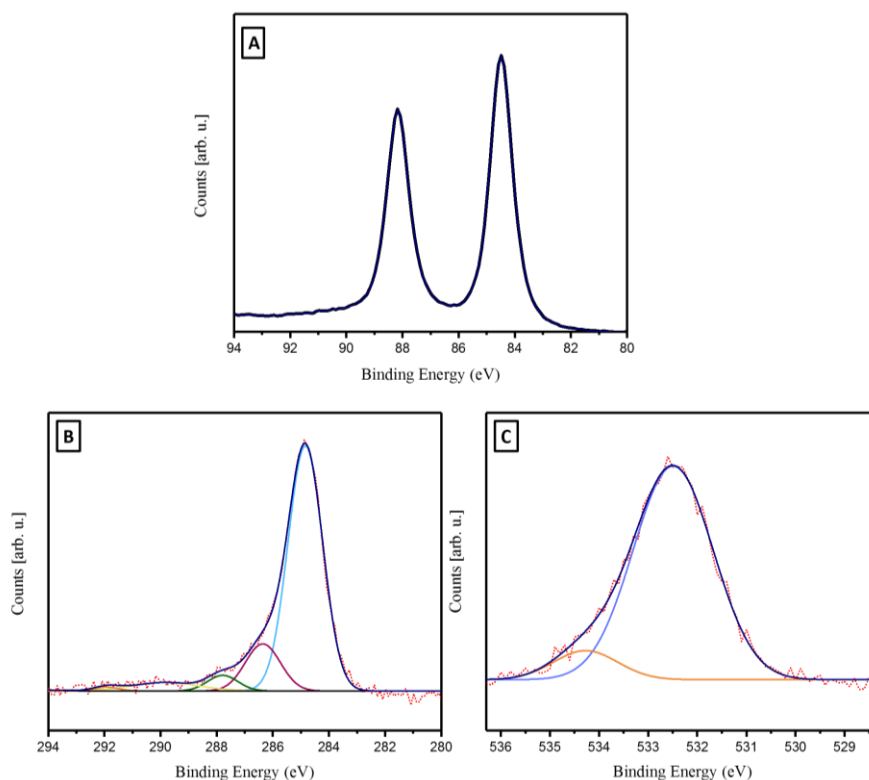
Figure 4.2. XPS spectrum of EAEA SAM on Au(111) substrate (A) Au 4f 7/2 peak (B) C 1s peak (C) O 1s peak.

The XPS spectra confirm the presence of different oxygenated products of the EAEA SAM. The oxygenated peaks are found at binding energies of 286.33, 287.89 and 289.80 indicating C-O, C=O, -COOH groups, respectively (Whelan et al., 2004). Deprotonation of the carboxyl group leads to a characteristic peak at ~288.2 eV in C 1s spectrum. The absence of this peak shows that there is no carboxylate formation. The XPS spectrum of the O 1s peak is shown in Figure 4.2(C). O 1s core level emissions of the EAEA SAM are observed at 533.62 eV and 532.16 eV, corresponding to hydroxyl and carbonyl oxygen atoms, respectively (Whelan et al., 2004). Jakhmola et al., observed that when the Au-O binding forms a carboxylate group an oxygen peak appears at 531 eV in the XPS spectrum (Jakhmola et al., 2017). The absence of this peak in our spectrum clearly demonstrated that the carboxylate group is not present in our EAEA SAM. The 292.11 eV binding energy peak, which is related to the $\pi \rightarrow \pi^*$ shake-up, has been observed for aromatic ring systems (Paul Pijpers and Meier 1999). Table 4.1 summarizes the XPS results. The area percentages of the various elements on the substrate are also shown. Table 4.1 shows the features for C 1s and O 1s by details and relative areas for carbon, oxygen and gold.

Table 4.1. XPS features, peaks and relative areas for C1s, O1s and Au4f of the EAEA SAM on Au(111)

Element	Carbon			Oxygen			Gold	
	Feature	**Position**	**%Area**	**Feature**	**Position**	**%Area**	**Position**	**%Area**
	sp^2	284.78	77.36				84.46	57.14
	C-O	286.33	11.19	C=O	532.16	86.82		
	C=O	287.89	6.17					
	-COOH	289.80	2.80					
	$\pi \rightarrow \pi^*$	292.11	2.48	-OH	533.62	13.18	88.13	42.86
Core Spectra	63.59±1.50			17.78±0.98			18.63±1.21	

PM-IRRAS measurements were performed in order to identify the various bonds that have been formed in the SAM. The PM-IRRAS results are compared with our XPS data. The complete IRRAS spectrum is depicted in Figure 4.3. The IRRAS technique has a high surface sensitivity, but we have to take into account the surface selection rules. According to the surface selection rules, only peaks that exhibit vibrational modes with

dipole moments perpendicular to the surface are visible. These peaks with a dipole moment perpendicular to the surface can interact with the incoming stationary electric field, whereas transitions with a dipole moment parallel to the surface are forbidden (Greenler 1966).

The IRRAS technique can also provide qualitative and quantitative information on the molecular orientation of the molecules by measuring the exact peak intensities (Li et al., 2014). PM-IRRAS signals of the EAEA SAM monolayer, which are shown in Figure 4.3, are in good agreement with results reported in the literature. All peaks in the spectra could be assigned by using data from the literature and the results are summarized in Table 4.1 and Table 4.2, respectively.
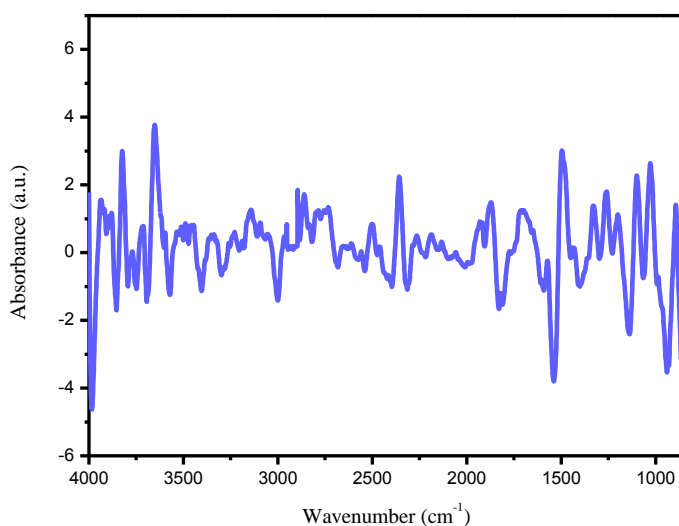
Figure 4.3. IRRAS spectrum of EAEA molecule on Au(111)

The alkyne ($-C \equiv C-$) band is located at 2157 cm^{-1} in Figure 4.4(A). Raman spectra results show that when the oligo(phenylene ethynylene)s (OPE) molecule binds to the gold substrate it has a red shift of about 200 cm^{-1} resulting in a shift from 2150 cm^{-1} to about 1950 cm^{-1}. These shifts demonstrate that the OPE molecules binds to the gold surface covalently as Au-C$\equiv$C- (Hong et al., 2012). However, it should be noted here that Nilsons et al., showed that free or weakly attached acetylenic groups resulted in a weak band between 2000-2200 cm^{-1} region for gold nanoparticles (Nilsson et al., 2007). An EAEA molecule contains two alkyne groups, where one alkyne group acts a spacer between two anthracene group and the other alkyne group serves as the end group of the EAEA molecule. The presence of the (-C$\equiv$C-) peak in the IRRAS spectra of the EAEA

SAM shows that the adsorbed monolayer still possesses an alkyne group that does not interact with the Au(111) surface. We anticipate that this weak peak arises from the spacer alkyne group of the EAEA molecule. Figure 4.4(B) shows the characteristic carbonyl stretching vibration υ(C=O) peak at 1713 cm^{-1}. The carbonyl peak has been found in the C 1s and O 1s XPS spectra.
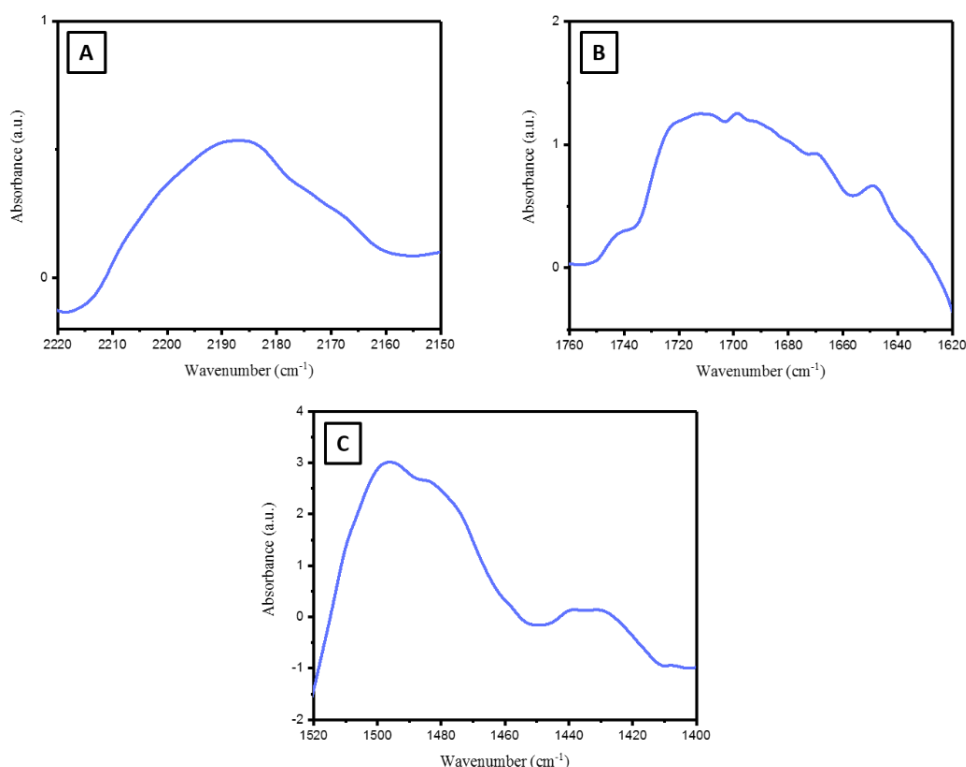
Figure 4.4. Vibrational modes of the as-prepared EAEA SAM measured by IRRAS (A) alkyne streching mode (B) C=O streching mode (C) Aromatic C=C streches region

The oxidation products which are observed in the IRRAS and XPS spectra are also expected because the experiments are conducted at ambient conditions. The characteristic peaks of the symmetric carboxylate stretch υ_s(COO$^-$) are, according to the literature, found at 1454 cm^{-1} and 1506 cm^{-1} , respectively (Pletincx et al., 2017). Both features were not observed in our IRRAS and XPS spectra. Figure 4.4(C) shows the aromatic C=C stretches, which is commonly observed for molecules having aromatic groups. These modes are located in ~1400-1600 cm^{-1} the region (Barriet et al., 2007).

To learn more about the oxidation products of the alkynes during monolayer formation, different regions of the IRRAS spectrum were analyzed with special attention for the carboxylate formation (Figure 4.5). The peak at 1330 cm^{-1} corresponds to the characteristic C-O-H bending mode (Figure 4.5(A)).

Table 4.2. IR vibrational frequencies (wavenumbers, cm^{-1}) obtained from EAEA molecule on Au(111) SAM formation by PM-IRRAS. The wavenumbers for the EAEA monolayer are compared with the literature in the second and third columns.

assignment	EAEA (cm^{-1})	Literature(cm^{-1})
(-C≡C-) stretch	2157-2164	2200-2000 (Nilsson et al., 2007)
(C=O) stretch	1713-1716	1710-1720 (Ramin et al., 2011)
(COH) bending	1331	1327 (Buchholz et al., 2016)
(OH) stretching	3651	3700 (Buchholz et al., 2016)
(CH) bending	1430	1431 (Rajalingam et al., 2010)
(CC) streching	1470-1500	1471-1571 (Barriet et al., 2007)

All peaks in the spectra were assigned by using data from the literature and the results are summarized in Table 4.2. The OH band was found at 3651 cm^{-1} for EAEA monolayer (Figure 4.5(B)). This result was also supported by the 1722 cm^{-1} IRRAS (Figure 4.4(B)) band, which reveals the presence of the carboxylic acid groups on the substrate.
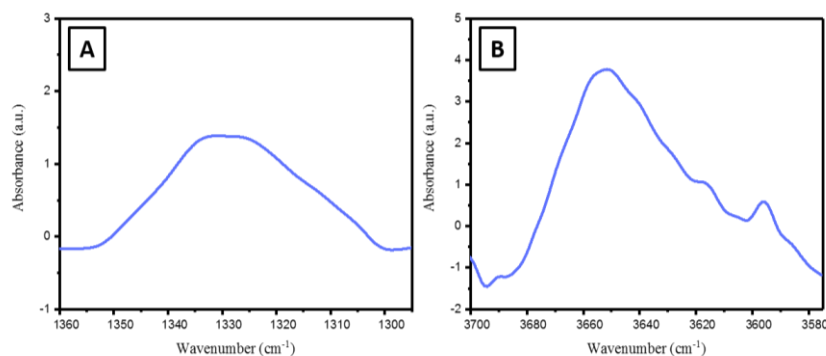
Figure 4.5. Vibrational frequencies of bands in EAEA SAM IRRAS spectra (A) COH bending modes (B) OH streching modes

According to the surface selection rule, only the vibrational modes that have a dipole moment perpendicular to the surface can be observed in IRRAS (Greenler 1966). The chain tilt angle can be calculated by analysing the IRRAS spectra (Du et al., 2005). In this study the tilt angle of the molecules was not determined. Qualitative information on the molecular orientation can be deduced from the absorption peaks. The intensities of the various groups in the spectra are quite different from each other. Figure 4.6 shows the mid to low region that can be assigned to the aromatic C-H and C-C vibrations. All the vibration modes are shown in Table 4.3.
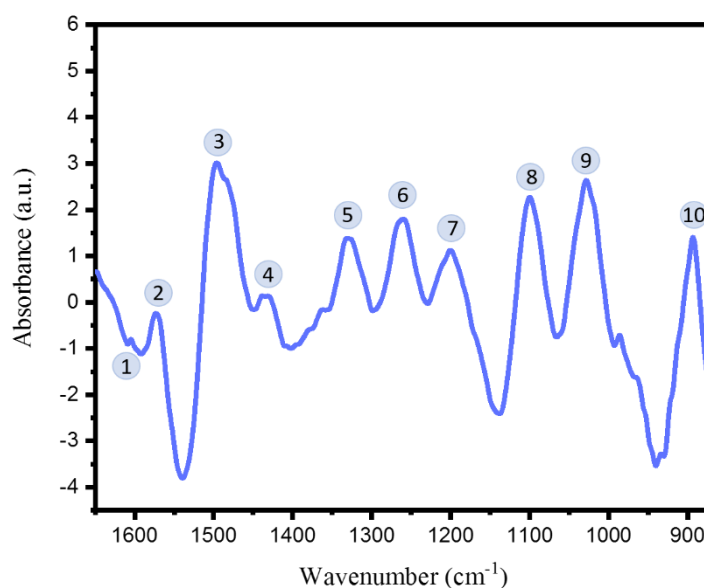
Figure 4.6. Mid to low regions IRRAS spectra of EAEA adsorbed monolayer on Au(111)

The modes labelled as 1, 2, 4 modes correspond to transition dipole moments (TDM) with are parallel and the 3, 5, 6, 8, 9 modes correspond to transition dipole moments which are perpendicular to the surface plane, respectively. The transition dipole moment for label 7 is neither exactly perpendicular, nor exactly parallel to the surface plane. The modes with perpendicular TDM refer to EAEA molecules that are nearly perpendicular to the substrate. If the modes which have a perpendicular TDM to the substrate had parallel TDM, the orientation of the EAEA monolayer would have been the upright configuration.

Figure 4.7 shows the oxidation products after the oxidation process of the EAEA molecule upon cleavage of the terminal and internal alkynes. This process leads to

breaking of carbon-carbon double or triple bonds and subsequent replacement by double bonds with oxygen (Vollhardt and Schore 2014). The possible products are carboxylic acids, acid anhydride and diketones. One of the proposed oxidation mechanisms results in the transformation of the alkyne end group in aldehyde and acid anhydride forms, which can be observed in the XPS spectra of both the C 1s and O 1s peaks. Also, in the IRRAS spectra one can find some evidence in favor of the XPS data. In the literature the reaction products of the alkynes have been studied at room temperature with are labelled acetylene (C_2D_2) and oxygen ($^{18}O_2$) molecules and the products have been reported as acetic acid and ketene, which are identified by using mass-spectrometry (Hay and Lyon 1970). Carboxylic acid has been found in the hydration product of the ketene, but further oxidation products have been determined as acetaldehyde functional group at 110 °C in a closed experimental system (Pritzkow and Rao 1985).

Both XPS and IRRAS data will help us to identify the oxidation products during the SAM formation of the EAEA molecules. Additional information on the oxidation can be obtained from the spectra of the alkyne (-C≡C-) groups (Zhang 2014).

Table 4.3. IR vibrational frequencies (wavenumbers, cm^{-1}) obtained for EAEA molecule. The assignenments is compared to the literature values (Source: Rajalingam et al., 2010, Käfer et al., 2006)

mode	(cm^{-1})	assignment
1	1604	CC_{ring} stretch
2	1572	CC_{ring} stretch
3	1496	CC_{ring} deformation
4	1438	CC_{ring} stretch
5	1330	CH_{ring} bending
6	1260	CH_{ring} bending
7	1200	CH_{ring} deformation
8	1100	CH_{ring} rocking
9	1028	CC_{ring} bending
10	893	CH_{ring} wagging

The expected atomic ratio between the carbon and oxygen atoms based on the molecular formula of the EAEA molecule was quite different from the experimental results as shown in Table 4.1. The atomic ratio between the C and O atoms was estimated to be 3.5:1 using our the XPS results. It should be noted here that only carboxylic acid formation results in a higher carbon amount as compared to the amount of oxygen. This result indicates that more oxidation products are formed, besides the aldehyde or carboxyclic acid.
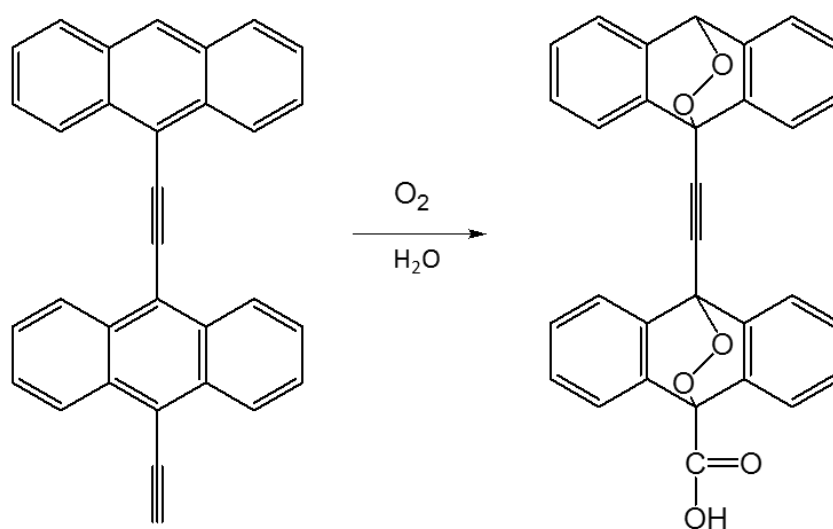
Figure 4.7. Feasible oxidation products mechanism for EAEA molecule by occurring carboxylic acid form of EAEA

Endoperoxide formation can explain the amount of the oxygen, which is known as a photooxidation product of anthracene (Wasserman et al., 2005, Parrish et al., 2012). The formation is depicted in Figure 4.7. The endoperoxide formations yields a ratio between the C and O atoms of 5:1. This result is consistent with our experimental results and therefore we believe that endoperoxide formation indeed occurs. The 286.33 eV peak may be attributed to endoperoxide formation (C-O bond formation).

Based on the ellipsometric measurements, contact angle, XPS and IRRAS analysis we have to conclude that the EAEA molecules chemisorb on the Au(111) surface. In contrast, Sotthewes et al., showed that air-exposed decanethiol molecules oxidized decanesulfonates only physisorbed on the Au(111) surface (Sotthewes et al., 2018). We tried to image oxidized EAEA molecules in order to obtain more information on the monolayer formation process. Figure 4.8 shows the high resolution scanning

tunnelling microscopy (STM) images of the ordered structure of chemisorbed EAEA molecules on Au(111). Figure 4.8(A) shows three irregularly shaped Au(111) terraces which are separated by monatomic steps. The step height between the different terraces was found to be monatomic in height, e.g. ~2.4 Å. The terraces represent an atomically flat Au(111) surface. Depression regions (darker spots) indicate vacancy islands, which occurs during the chemisorption of the molecules due to the rearrangement of the gold surface atoms (Noh and Hara 2001). The depth of the vacancy island is equal to one atomic layer (2.4 Å), which is also described as etch-pits formation (Bose and Yoshitake 2005). The observed etch pits are therefore not holes in SAM, but rather vacancy islands in the Au(111) surface.

Also observed etch-pits were reported as a characteristic of attached aromatic moieties from the head group to the gold substrate (Yang and Liu 2003). The Au(111) surface exhibits, besides flat regions also one atomic layer high (or deep) small islands and vacancy islands, see Figure 4.8(B). A statistical analysis reveals that the EAEA monolayer has a 43% surface coverage. In Figure 4.8(C) the SAM shows up as bright, but flat regions. Etched pits formation is observed on the terraces, the defects are hardly seen in the ordered structure, but can be resolved in smaller scale STM images; see Figure 4.8(D).

The STM images exhibit both short-range and long-range ordering of the SAM. The long-range SAM formation, which is rarely seen for the alkyne ligand-Au(111) interaction shows up in Figure 4.8(C) in a large domain of about 405 nm^2, but also various smaller sized SAM islands were found between 70 nm^2 to 15 nm^2 (Figure 4.8(B)). McDonagh et al., showed that the ethynylbenzene molecules have short-range order on Au(111) substrate and bind to the substrate via the carbon atoms (McDonagh et al., 2007).

DFT modelling was used to understand the lattice structure of the EAEA SAM (Figure 4.9) with the very much appreciated support from our colleague Tabassom Arjmand. The most noticeable point is the rotation between the two anthryl groups of the molecules from the top (Figure 4.9(A)) and side view (Figure 4.9(B)) of the molecules. The rotation of the top anthryl occurs at the acetylene linkers (Toyota et al., 2010). The acetylenic axis of the aromatic system has been used to construct the model by decreasing the freedom of motion. Dihedral angles θ represents the rotating angle of the molecule with respect to the acetylene spacer. The rotation can be restricted by steric effects. The dihedral angle as observed in STM images amounts θ=30°. DFT modelling also reveals

the rotation of the acetylene linkers axes, which will of course affect the molecular structure and ordered structure of the SAM formation.

The ordered monolayer structure was confirmed by Fourier spectrum, which shows a parallelogram lattice, see FFT spectrum in Figure 4.10(A). The hexagonal FFT lattice is clearly seen in Figure 4.10(B). Due to the limited resolution the details of the structure cannot be resolved.
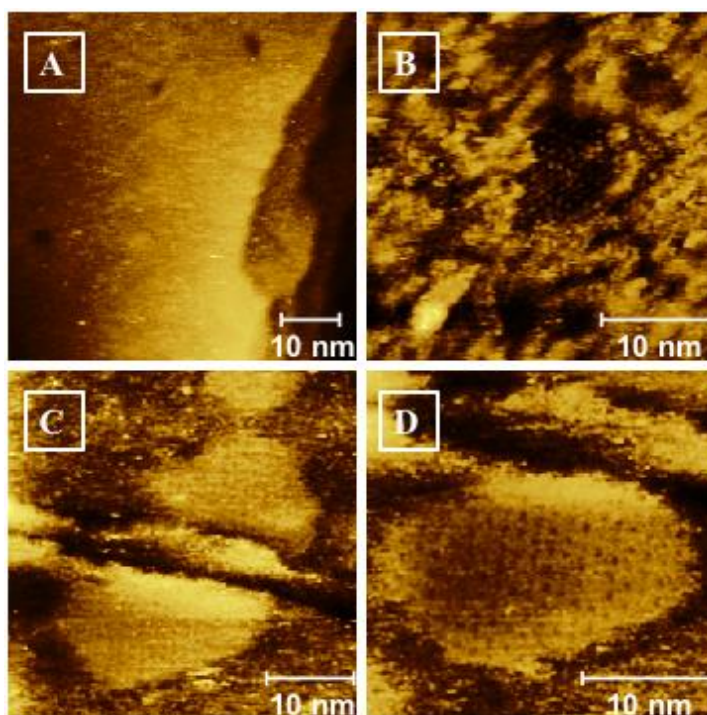
Figure 4.8.   (A-D) High resolution STM topographical images were obtained from different regions and scales on Au(111) surface. These images are taken at a sample bias voltage of 220 mV and a tunnelling current of 230 pA.
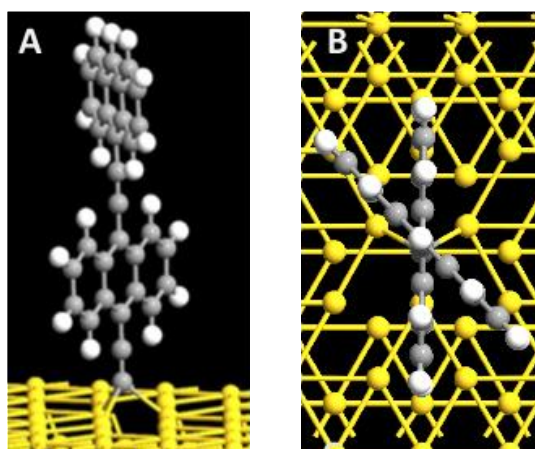
Figure 4.9. (A) Side view model of EAEA molecules on Au(111) (B) Top view of the EAEA molecule (DFT modelling on Au(111)).
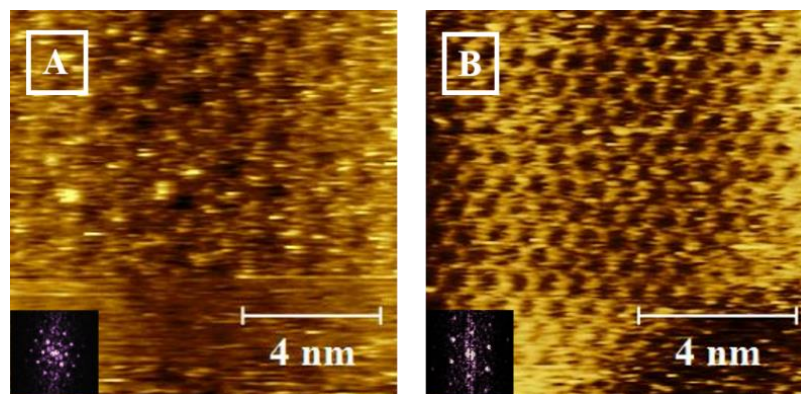
Figure 4.10. (A) Topographic image of EAEA SAM , tunnelling current 150 pA, sample bias 150 mV, scale bar 2 nm. Inset in (A) FFT spectrum of the STM image showing a two-fold symmetry (parallelogram). (B) High resolution Topographic image of the EAEA SAM on Au(111), tunnelling current 230 pA, sample bias 220 mV, scale bar 2 nm. Inset in (B) shows FFT spectrum of the image with 6-fold symmetry.

The information on the molecular orientation given by IRRAS spectra reveals that the EAEA are slightly tilted on the Au(111) surface. More insight regarding this tilting can be obtained by DFT calculations. The orange and blue rectangular shapes show the top and bottom anthryl part of the molecule respectively. The model reflects the main features of the SAM ordered structure (see FFT image and Figure 4.11(A)). The possible binding positions for the molecules on Au(111) substrate are; the top site, the bridge site, the hcp hollow site and the fcc hollow site (Zhang et al., 2002). Former studies have shown that the most energetically favourable position for alkyne end group molecules is at the fcc lattice site via σ bonding between the C and Au atoms forming a perpendicular orientated bond (Tang and Jiang 2014). The proposed model is schematically shown in Figure 4.12. The rotation angle between the two anthryl groups was found to be 36°, which should be compared to the 30° rotation found by DFT modelling. The line profile, which is shown in Figure 4.11(1-2-3) exhibits a distinct height difference between the dim and bright parts of the STM images. These height differences may arise from the top and bottom anthryl groups, see the model structure. The lattice is consistent with a $3\sqrt{2}a$ unit cell for the monolayer structure. The unit cell of the alkyne SAMs is different than the unit cell of the alkanethiol based SAMs The reason for the rotation of the anthryl groups is due to a reduction of the surface energy upon adsorption of the molecule on the Au(111) substrate. The anthryl groups were rotated to maximize the $\pi - \pi$ interactions (Dou et al., 2006). The parallel displacement contributes to the turning of the top anthryl

part from the carbon atom which binds to the acetylene spacer at a certain angle. Rigid molecules inhibit a free rotation from the acetylene axes. Based on our experimental observations and DFT calculations we determine this rotation to be about 30°-36°.
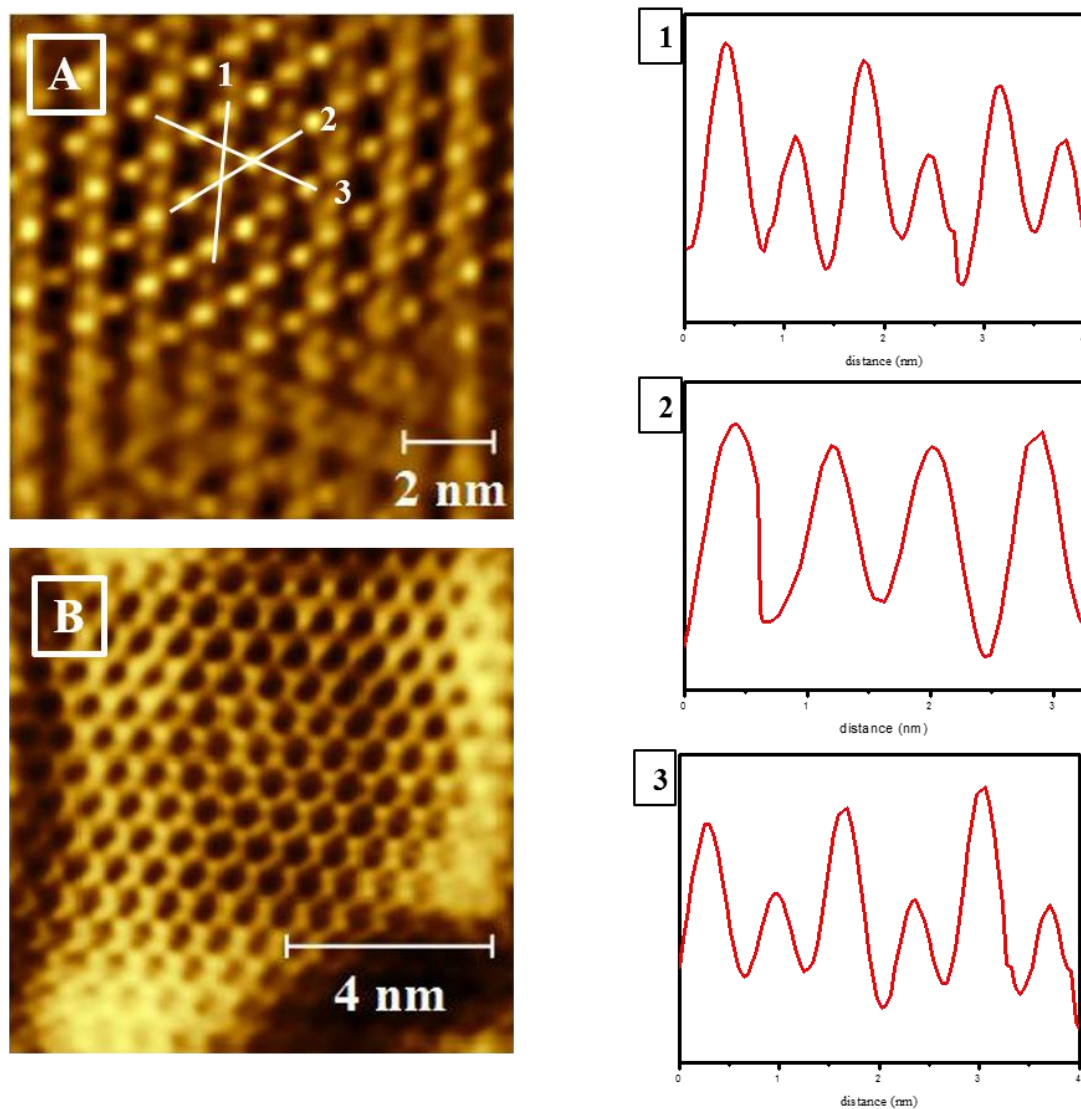
Figure 4.11. (A) FFT filtered image of image 4.11. (A), (B) FFT filtered image of image 4.11. (B), (1-2-3) line profiles indicated in (A).

The electronic properties of the ordered SAM structure of EAEA molecules adsorbed onto Au(111) were measured by scanning tunnelling spectroscopy (STS). The I/V curves recorded on the EAEA SAM show a semiconducting behaviour (Figure 4.13). The energy gap between the highest occupied molecular orbital and the lowest

unoccupied molecular orbital was measured to be ~1.4 eV (200 pA). Local density of states (LDOS) were obtained for the EAEA SAM by differentiating the I(V) spectra.
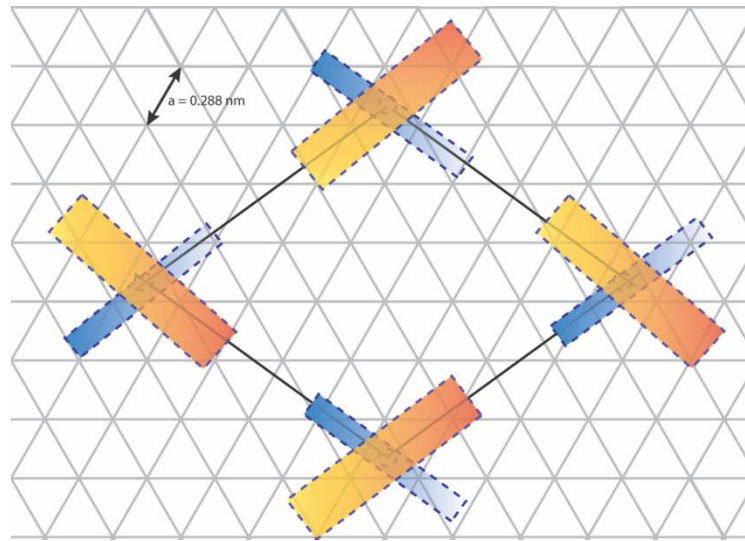
Figure 4.12.   The proposed model for the EAEA molecules on the Au(111) substrate.
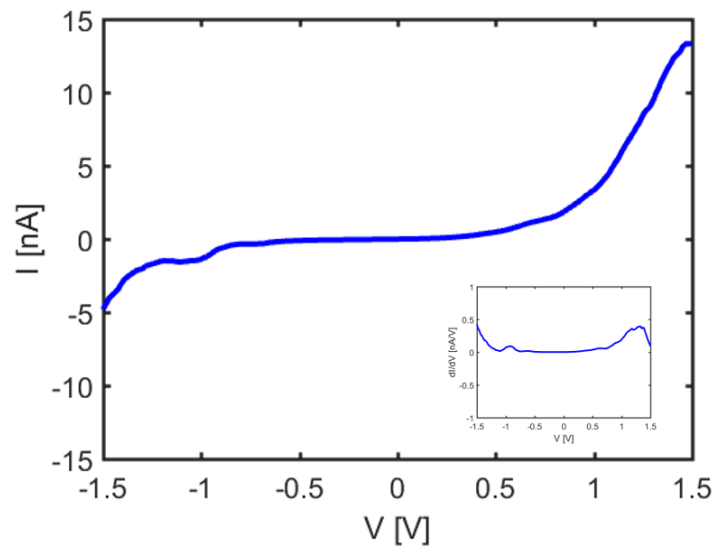
Figure 4.13. Current-voltage characteristic of the EAEA SAM on Au(111). The inset shows the dI/dV characteristics of the system. The STS was obtained with a sample bias voltage ranging from -1.5 V to 1.5 V and a tunnelling current of 200 pA.

The differential tunneling conductance, dI/dV, which is proportional to the LDOS, is shown in the inset of the Figure 4.13. The voltage interval was chosen from -1.5 and

+1.5 V, in order to obtain an accurate local density of states of the SAM near the Fermi level. The existence of a band gap reveals that the EAEA molecules are indeed adsorbed on the Au(111) substrate. The bare Au(111) is gapless and has an almost linear I(V) curve.

The measured IRRAS and XPS peaks clearly show that the EAEA molecules are oxidized on the Au(111) surface. The etched pit formation which is very characteristic feature in the formation of SAMs, indicates that a EAEA SAM has formed. This conclusion is reinforced by STS experiments, which clearly revealed the opening of a band gap. Our experimental findings regarding the orientation and structure of EAEA upon adsorption on the Au(111) surface are supported by DFT calculations.

4.6. Conclusion

In this study SAMs of EAEA molecules were investigated with STM, XPS, IRRAS and STS. The exposure of EAEA molecules to Au(111) at ambient conditions affect the oxidation by opening of the C-C triple bond of the alkyne end groups which leads to different oxidation products observed in XPS and IRRAS. STM and STS data provide strong evidence for chemical bonding. The STM images show ordered structures within different sized domains of the SAM. The Au(111) herringbone reconstruction was not observed indicating that the interaction between the molecules and the Au(111) surface is rather strong. The rearrangement of the EAEA molecules is obtained by a combination of the acetylene linker rotation, the parallel-displaced $\pi - \pi$ stacking intermolecular interactions and the preferred fcc hollow adsorption site. The spacer increases the flexibility of the molecule, which allows the molecule to find its lowest energy configuration via the optimization of interactions with nearest-neighbour molecules. This eventually leads to well-ordered domains with low defect concentrations, at least as compared to molecules without a spacer group (Dou et al., 2006). Our results reveal that conjugated pi systems and the acetylene linker increases the ordering of the SAM. STS results show the presence of the molecules due to the existence of a band gap. The oxidation products of the EAEA molecule do not affect the binding properties. We have found that the carbon atom of the EAEA molecule binds to the Au(111) surface. In contrast to this system we found in Chapter 3 that the oxidized alkanethiol molecules transform into the sulfonates molecules by physically interacting with the substrate. Here the oxidized alkyne end group molecules are still chemically bonded to the Au(111)

substrate making these system very suitable for ambient condition technological applications. Our experimental results are very useful for future investigations of SAMs containing an alkyne end group. We anticipate that our results will help to improve the understanding of (1) the interaction with the Au(111) substrate and (2) the oxidation of the EAEA molecule.

CHAPTER 5

MOLECULAR STRUCTURE AND BINDING PROPERTIES OF SELF-ORGANIZED MONOLAYER A RUTHENIUM(II) DYE COMPLEX ON AU(111)

5.1. Introduction

Self-assembled monolayers (SAMs) are effective and convenient structures for preparing ultra-flat highly ordered structures on gold that be utilized in application as electrochemical sensing (Chen and Li 2006), molecular electronics (Atesci et al., 2018) and biomolecular investigations (Senaratne et al., 2005). The growing interest on ruthenium complexes arises from the photoactive properties leading to new applications such as cell imaging (Rogers et al., 2014) and redox active surfaces (Eckermann et al., 2010). Easy fabrication and interface manipulation make SAMs an appealing route method to improve new applications by using, for instance, the chemical properties of ruthenium based photosensitive molecules. In the recent years Ru(II) dye molecules have been used to characterize on TiO_2 and Au(111) (McFarland and Tang 2003) substrates which are used as electrode materials for dye-sensitized solar cells (DSCs). The conversion efficiency is affected by charge transfer properties which are altered by adsorption geometry of adsorbed dye molecules on substrate (Hauptmann et al., 2013). Ru(II) dye molecules have two carboxylic (bi-isonicotinic and two thiocynate) groups on its structure, which are the possible binding groups for Au(111) surface. The N3 molecule which is mostly used in DSCs is also a Ru(II) dye complex, and has been investigated on TiO_2 substrate. Bonding occurs via oxygen atoms by deprotonation of the carboxylic acid ligands to the surface (Schnadt et al., 2002). Binding affinity of the N3 molecule has been studied on Au(111) substrate. It has been shown that sulfur atoms covalently bond to the gold surface and the bi-isonicotinic acid is only physisorbed to the Au surface (Mayor et al., 2009).

CS28 molecules have been synthesized as a type of next generation solar cells to respond the demand of the DSSCs conversion efficiency. The designed structure has an

alkyl substituent in order to avoid problems like aggregation and water adsorption of the dye molecule. The molecules have $\pi \rightarrow \pi^*$ transition in bipyridine and pyridine ligands at 299 nm and 370 nm main peaks (Sygkridou et al., 2015) addressing the molecule as a photoactive SAM structure.

The CS28 forms a self-assembled monolayers on Au(111) substrates. The combination of advanced techniques, such as scanning tunneling microscopy (STM) and X-Ray photoelectron spectroscopy (XPS), are combined with electrochemical-based techniques in order to study the structural and electronic properties of CS28 SAMs. In this work electrochemical techniques such as electrochemical impedance spectroscopy (EIS) and cyclic voltammetry (CV) have been used to investigate the interfacial properties in presence of the $Fe(CN)_6^{3-/4-}$ external redox. Experiments show that CS28 binds to the Au substrate via sulfur atoms. The CS28 SAM exhibits a higher resistance than the bare Au(111) substrate.

5.2 Experimental Methods

5.2.1. Materials

The solvents were obtained from commercially and used without any further purification. Au(111) films on substrate have been purchased from Phasis, Switzerland. The Au films have a thickness of 150 nm. The following chemicals have been used: N-N Dimethylformamide (DMF) (>99%, Aldrich), 2- propanol (Merck , for analysis), H_2O_2 (Aldrich 34,5-36,5%), H_2SO_4 (95-97%, Aldrich), pure water (Merck Millipore), KOH (>99.97, Sigma-Aldrich).

5.2.2. Preparation of Self-Assembled Monolayers

SAMs were prepared by immersing the Au(111) substrate into 0.1 mM CS28 molecules (Figure 5.1.) DMF solution. The glass tube was sealed and kept 24 h at 60 $^{\circ}$C. All glassware was immersed before using sequentially in a fresh acidic piranha solution (H_2O_2/H_2SO_4, 3:7, v/v) and a basic piranha solution (H_2O_2/KOH/2-propanol, 15:15:1, v/v). Subsequently the glassware was rinsed several times with ultrapure Milli-Q water. contaminants and atmospheric carbon. The Au(111) substrate was removed from the

solution and rinsed with copious amounts of solvent and dried by N_2 gas at room temperature. These treatments removed any surface
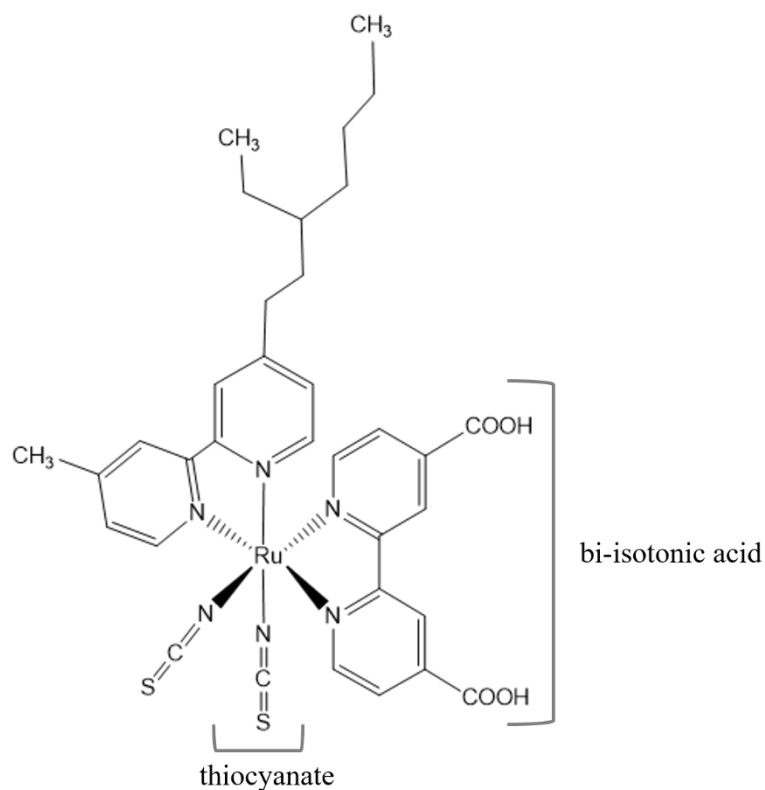
Figure 5.1. Molecular structure of the ruthenium(II) complexes.

5.2.3. XPS Measurements

XPS data were recorded with a PHI Quentera SXM photoelectron spectrometer. The Al Kα-radiation was used to obtain the XP spectra of SAMs (spot size 200 μm). The spectra were recorded in constant analyser energy (CAE) mode with analyser path energies of 150 eV for the survey spectra and 1000 eV for high-resolution spectra.

5.2.4. Scanning Tunneling Microscopy

STM imaging was conducted with a Nanosurf Easy Scan 2 system at ambient conditions and at room temperature. Imaging was performed in the constant current mode using tunnelling currents between 250 and 280 pA and bias voltages between 0.7 and 0.5

V, respectively. The STM piezo's were calibrated by measuring the surface lattice constant and step height of a freshly cleaved graphite surface.

5.2.5. Electrochemical Measurements

Cyclic voltammetry measurements were achieved with an AUTOLAB PGSTAT10 in the voltage range from -1 to 1 V. The measurements have been performed on bare Au(111) and CS28 modified Au(111) substrates. An electrochemical cell with ~1.4 cm^2 probe area was used. Ag/AgCl was used as a reference electrode and a Pt wire as a counter electrode. The electrolyte consisted of a 3 mM potassiumhexaferrocyanide (II), $K_4Fe(CN)_6$ in 1 M K_2SO_4 as supported electrolyte in aqueous solution, and the scan rate was 100 mV/s. For impedance spectroscopy measurements, measured frequency range was 0.1 Hz-50 kHz.

5.3 Results and Discussion

The electrochemical properties of self-assembled monolayers on metal substrates has been studied by several research groups (García-Raya et al., 2008). The structural information has been gathered by varying the kinetics of the electron transfer reaction in the presence of SAM formation (Ding et al., 2005). Cyclic voltammetry method is the most commonly used method to determine blocking effects of modified electrodes. Figure 5.2 shows the CV measurements which were performed on bare Au(111) and CS28 modified Au(111) substrates.

A monolayer coated Au(111) substrate and a redox couple are used as electrodes for cyclic voltammetry measurements. The electrochemical behavior of CS28 SAM was investigated with 3 mM $Fe(CN)_6^{3-/4-}$ redox couple on Au(111), which was used as a working electrode. The electron transfer is brought about by a tunneling process, permeation of redox species to gold surface or via pinholes and defect sites (Amatore, Savéant, and Tessier 1983). During the scanning of the sufficiently positive potential the $Fe(CN)_6^{4-}$ is oxidized, the anodic current occurs by the reaction;

$$Fe(CN)_6^{4-} \rightarrow Fe(CN)_6^{3-} + e- \qquad (5.1)$$
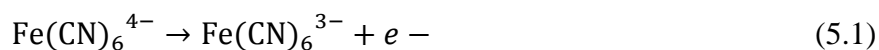
The SAM formation on Au(111) working electrode acts as an oxidant and the oxidation current starts to increase until there is a maximum on the peak. The concentration of the $Fe(CN)_6^{4-}$ redox reactant starts to decrease, resulting in the depletion of the SAM modified Au(111) surface and the current decreases. At the negative voltage region the potential is high enough to oxidize $Fe(CN)_6^{4-}$ species. The gold electrode becomes strongly reductant and an a layer as $Fe(CN)_6^{3-}$ is formed by the reaction;

$$Fe(CN)_6^{3-} + e^- \rightarrow Fe(CN)_6^{4-} - \qquad (5.2)$$
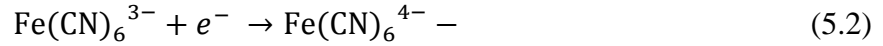
resulting in a cathodic current, until the $Fe(CN)_6^{3-}$ in the solution is consumed. Oxidation occurs towards the forward scanning and $Fe(CN)_6^{3-}$ oxidizes to $Fe(CN)_6^{4-}$ (anodic process) and reverse scan allows to generate $Fe(CN)_6^{4-}$ by reducing $Fe(CN)_6^{-3}$ during the cathodic process. Bare Au(111) surface shows a quasi-reversible behavior, which indicates the oxidation and reduction processes occurring at slightly different potentials for $Fe(CN)_6^{3-/4-}$ redox couple with a peak potential separation, 290 mV, which is inversely proportional to the electron transfer rate (Harris and Bruening 2000) (ΔE_p is around the potential difference between the oxidation peak potential and reduction peak potential). For a totally reversible reaction peak the separation potential should have been $\Delta Ep=56.5/n$ mV at 25 ^oC (Bard et al., 1980). However, the peak potential separation for the CS28 modified gold surface between the anodic and cathodic peaks are compared with the bare Au(111) surface. This result reveals that the electron transfer rate is lower for modified gold surface than for the bare gold surface.

The surface blockage is effective and the electron transfer is inhibited by the monolayer. The peak current also decreases for CS28 modified Au(111) substrate as compared to bare substrate, indicating the $Fe(CN)_6^{3-/4-}$ redox couple inhibition in the electrochemical process. Thus, a barrier is formed which inhibits the electron transfer reaction and the electron transfer occurs via ´pinholes´ at the electrode surface (García-Raya et al., 2008).

The sample was placed in the cell in a 0.1 M K_2SO_4-$Fe(CN)_6^{3-/4-}$ redox couple in water solution. The redox couple is able to sense the electrochemical activity of the SAM formation on Au(111) (Pissinis et al., 2014). Data were gathered with 100 mV/s scan rates between +800 and -200 mV to avoid desorption of the SAM. All recorded data are averages of four scans. $Fe(CN)_6^{3-/4-}$ was selected owing to its reversibility in electrochemical environment.
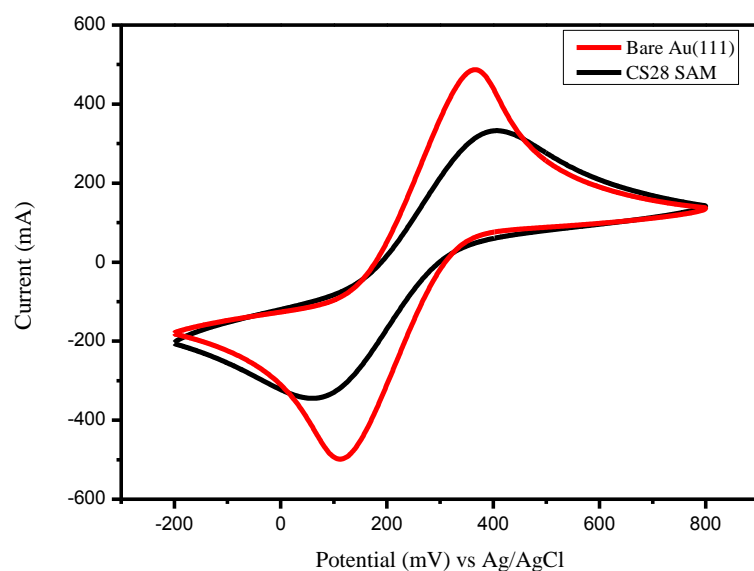
Figure 5.2. Cyclic voltammograms of 3mM $Fe(CN)_6^{3-/4-}$ in 1 M K_2SO_4 aqueous solution at (−) bare Au(111) and at (−) CS28 modified Au(111). Scan rate 100 mV/s.

Impedance spectroscopy is a powerful method to investigate the charge transfer process of the modified electrode. An ac impedance method has been used that measures the response of the electrochemical system with a small-amplitude alternating potential. Figure 5.3 shows the Nquist diagrams of the impedance results obtained from a 3 mM $Fe^{2+/3+}$ + 0.1 M K_2SO_4 solution for the bare Au(111) substrate and CS28 modified SAM. Randles equivalent electrical circuit usually represents the measured system (Nicholson and Shain 1964). The impedance plot is given in the low frequency and high frequency regions in the frequency domain 0.1 Hz to 50 kHz. The bare Au(111) substrate has a low frequency straight line following a small semicircle at high frequency corresponding to a diffusion controlled process for the redox couple. A straight line is found at low frequency region and the blocking is not present at the bare Au(111) surface. Smaller semicircular diameters, which is related to the charge transfer process, demonstrated a faster electron kinetics of $Fe(CN)_6^{3-/4-}$ on bare Au(111) (Mendes et al., 2004). The Nyquist plot obtained from CS28 monolayers shows a semicircle with high-frequency region. The heterogeneous charge-transfer resistance increases due to the inhibition of electron transfer rate by CS28 monolayer. When an electrode is modified with the SAM there is a decrease in the current as compared to non-modified electrode (Ding et al., 2005). The difference arises from the effective blocking property of the CS28 SAMs related to the redox reaction of $Fe(CN)_6^{3-/4-}$ at the Au(111) electrode. A straight line was not observed at the low frequency region for CS28 modified gold surface when the pinholes and defects

are far away from each other.   Only in the situation that neighboring pinholes overlap each other, it is possible to observe straight lines at the low frequency region.
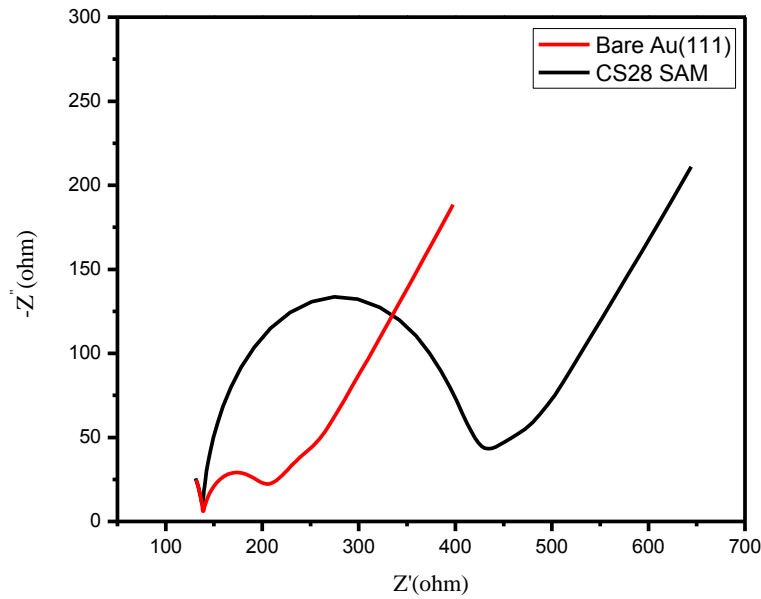
Figure 5.3. Nyquist diagram of 3mM $Fe(CN)_6^{3-/4-}$ in 1 M K_2SO_4 aqueous solution at (−) bare Au(111) and at (−) CS28 modified Au(111)

The coverage (θ) of the Au(111) can be estimated by using the resistance values of the charge transfer for Au(111) and SAM modified surface. Practically, SAM formation inhibits the charge transfer, however, surface imperfections and pinholes allow molecules and ions of the electrolyte to reach the electrode surface (Campuzano et al., 2006). Pinholes, which are consisted of defects are caused by imperfect adsorption during SAM formation or caused by losing molecules during the SAM rinsing process or during storage (Deligianni 2010). The coverage can be calculated presuming that all the current is passed through pinholes of the Au(111) electrode using equation 5.3.

$$(1 - \theta) = R_{ct}{}^0 / R_{ct} \tag{5.3}$$

$R_{ct}{}^0$ is the charge- transfer resistance at bare Au(111), R_{ct} is charge-transfer resistance CS28 modified Au(111) electrodes under the same conditions. The R_{ct} value which is obtained from the the diameter of semicircle for the CS28 monolayer covered electrode is greater than $R_{ct}{}^0$ due to the blockage of the electrode by the CS28 SAMs.
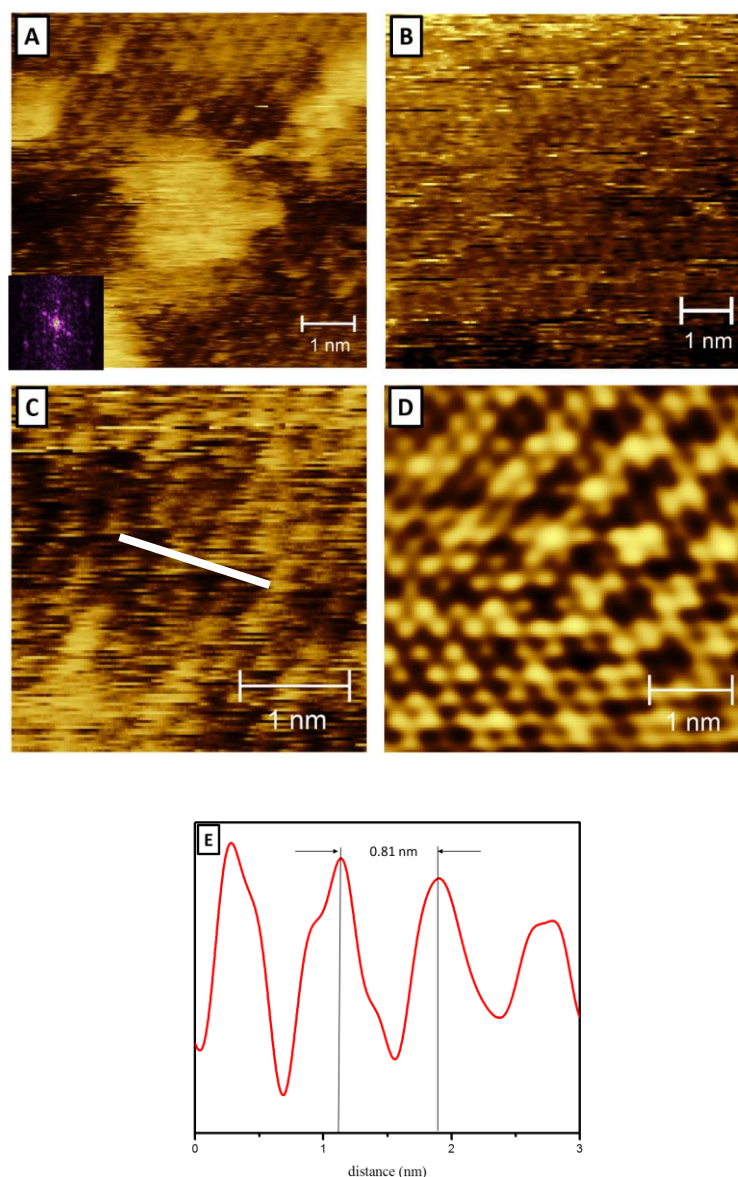
Figure 5.4. (A) Topographic image of CS28 SAM , tunnelling current 272 pA, sample bias 500 mV, scale bar 1 nm. Inset in (A) FFT spectrum of CS28 molecules STM image (B-C) small scale topographic image of the CS28 SAM on Au(111) (D) shows FFT filtered image CS28 SAM surface (E) line profile indicated in (C).

The charge transfer resistance , $R_{ct}{}^{0}$ and , R_{ct} was found to be 101 Ω cm^2 and 207 Ω cm^2, respectively. The coverage was found as 0.51 for low concentration (5 µM) SAM preparation. The pinholes, SAM formation and Au(111) features were observed by using scanning tunneling microscopy (STM).

Figure 5.4 shows the STM images of CS28 SAM (on Au(111) surface). The ordered structure is seen in the images and six-fold symmetry is observed after FFT

filtering. The bright protrusion on Figure 5.4(A) refer to some disordered molecules on the bare gold surfaces. Figure 5.4(A) and (B) shows small scale images of CS28 deposited Au(111) surfaces. The surface was covered with parallel stripes. The spacing between the nearest neighboring stripes were determined by a cross-section of the line (Figure 5.4(C)) and is 0.81 nm. The STM image in Figure 5.4(D) results from Fourier transform filtering of ordered parallel stripes. Ru(II) complexes were studied by diazonium electroreduction method on HOPG substrates and parallel stripe formation was observed by a cross-section of 3.8 nm which matched the molecular length of the molecule (Nguyen et al., 2016).
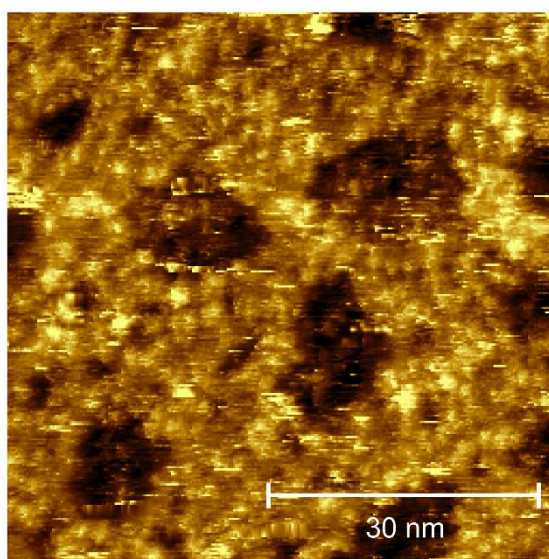
30 nm

Figure 5.5. Large-scale STM image for CS28 SAM structure on Au(111) tunnelling current 250 pA, sample bias 700 mV, scale bar 30 nm.

Figure 5.5 shows an STM image of a large area with a low molecular coverage, which has defects such etch-pit formation (also known as vacancy islands) and pinholes in the substrate, which may arise from the surface reconstruction by chemical bonding between the substrate and molecule (Brown et al., 2011). The long-range ordered orientation was not observed on the large-scale image. n-alkanethiol molecules prefer to adsorb at fcc lattice sites of the Au(111) substrate and occupy these sites since it gives the lowest surface energy per unit area. The molecules can also adsorb at different locations, which destroys the long-range order (Katsonis et al., 2003).

X-Ray photoelectron spectroscopy (XPS) measurements were performed on the CS28 modified monolayer. The XPS survey scans showed the presence of gold, carbon, nitrogen and sulfur. Figure 5.6 indicates XP spectra (A) C 1s (B) N 1s (C) O 1s and (D)

S 2p. C 1s peaks are indicate ~285 eV pyridine rings as the most intense peak. Two of peaks have equal intensity (located at 285.19 eV and 284.80 eV binding energies). The difference arises from N binded C atoms (Mayor et al., 2009). The aliphatic C 1s peak is seen at 284.41 eV, and the carboxyl C 1s peak on 288.82 eV. The remaining C 1s feature at 287.96 eV indicates the presence of thiocynate C atoms. The thiocynate N 1s XPS peak has two binding energy peaks at 398.00 eV and 397.18 eV, which is a strong evidence that binding occurs at one of the sulfur atoms of the thiocynate groups. The chemical bonding between the sulfur and gold has been shifted to lower binding energy for N 1s. The N 1s spectrum corresponds to the N atoms, which are located in the phenyl rings around 400 eV binding energies.

The binding properties are also obtained from S 2p XPS peak, as can be seen in Figure 5.6(C). There are three mean peaks at 161.19 eV, 162.91 eV and 163.16 eV binding energies corresponding to bonded, nonbonded and dimerized bonded S atoms to the Au(111) surface (Mayor et al., 2009, Fenter et al., 1994). DFT calculations showed that ruthenium dye N3 (cis-Bis(isothiocyanato)bis(2,2′-bipyridyl-4,4′-dicarboxylato)ruthenium(II) molecule are adsorbed on to the Au(111) surface via S atoms of isothiocyanate groups (Hauptmann et al., 2013).

The binding of COOH groups at the Au(111) substrate is also possible. O 1s XPS peaks were found around 531.80 eV and 532.59 eV, which indicate to carbonyl (C=O) and hydroxyl (C-OH) features, respectively. The oxygen atoms may interact with the Au(111) substrate if the O atoms are deprotonated under certain conditions. SERS results showed that the carboxylate group has no interaction with the surface, and adsorption occurred from the thiol group which is covalently bound to Au(111) surface in the case that strong alkaline aqueous solution (pH~13) were used. However, in acidic solutions strong interactions of carboxylate group took place on the gold surface (Pissinis et al., 2014). Deprotonation of the carboxylate was expected at lower pH values due to the deprotonation, which hinders the electron transfer (Mendes et al., 2004). In the prepared solvent of the CS28 solution in DMF (pH value of 6.5) XPS results also revealed that oxygen is protonated (for carboxylate groups).
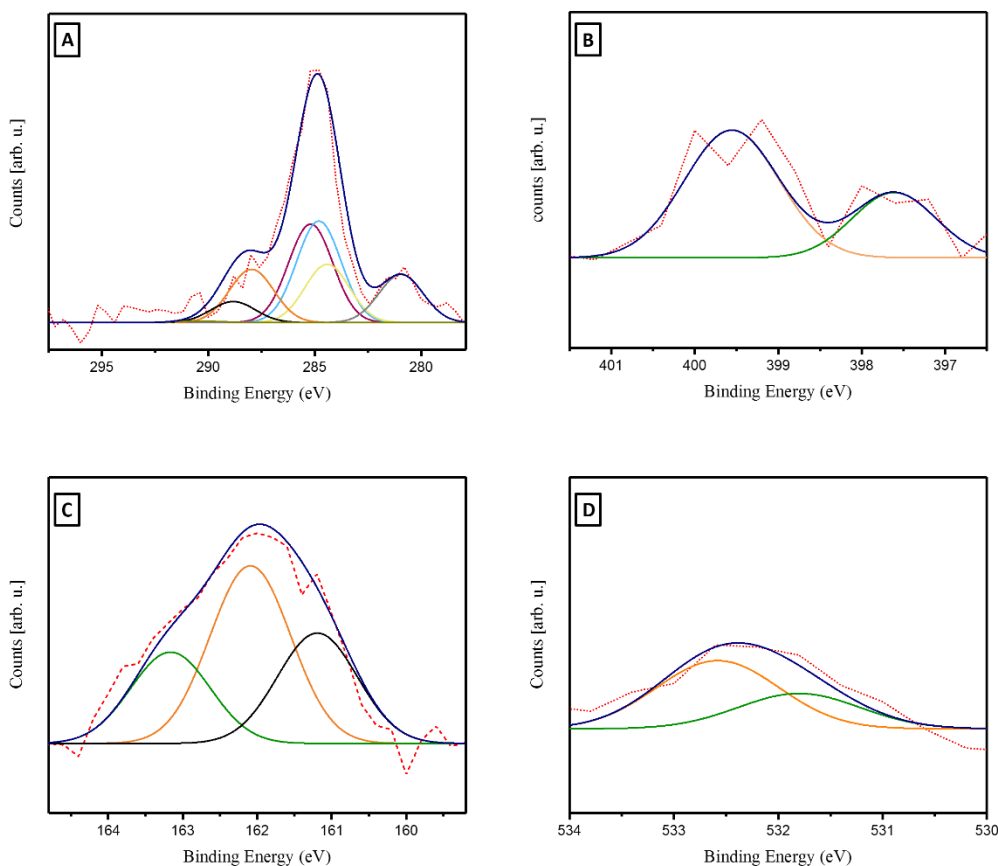
Figure 5.6. XPS spectrum of CS28 SAM on Au(111) substrate (A) C 1s (B) N 1s (C) S 2p (E) O 1s

5.4 Conclusion

In this study, Ru(II) complex, with CS28 have been investigated for the first time. We found a the formation of a SAM on the Au(111) surface. The SAM surface was characterized by electrochemical cyclic voltammetry and impedance spectroscopy, STM and XPS methods. Current electrochemical measurements, cyclic voltammetry and impedance spectroscopy, revealed that the $Fe(CN)^{3-/4-}$ redox reactions on the gold surface were blocked in the CS28 SAM as compared to the bare Au(111) substrate. The defects, such as pinholes, vacancies, etched pits decrease the resistance of charge transfer of the SAM and allow the access of ions to the substrate (Campuzano et al., 2006). The surface coverage can be estimated by the EIS measurements, which was found to be %51 SAM coverage on Au(111) surface. The quasi-reversible voltammogram shape can be explained by the low coverage SAM formation on Au(111) surface. The complex

molecule in the monolayer has a locally long-range organized order which is observed by STM. The spacing between the parallel stripes is 0.81 nm, which is a sign of the ordered packing structure. With the help of STM and XPS, the molecular structure and binding properties of the CS28 molecules were studied. This provides a deeper insight into carboxyl and sulfur groups binding affinity to Au(111) substrate. This new SAM system will help us to look for new possibilities and the improvement in applications such as photosensitive molecules, photoactive surfaces and sensors and new photonic application of dye-sensitized solar cell molecules. It will also contribute to a better understanding of the preparation of high quality monolayers.

CHAPTER 6

CONCLUSION

The self-assembled monolayers (SAMs) have attracted enormous attention due to their interesting physical and chemical properties on solid surfaces. The application of the SAMs critically depends on their structural, electronic and dynamic properties. For this reason, it is important to study the ordering properties, electronic properties and dynamic processes on surfaces. This work deals with the comparison of alkanethiol and alkyne SAMs formation on Au(111) surfaces by using mainly scanning probe microscopy techniques, such as scanning tunnelling microscopy (STM), scanning tunnelling spectroscopy (STS) and time-resolved scanning tunnelling microscopy (TR-STM), X-Ray photoelectron spectroscopy (XPS) and infrared-reflection absorption spectroscopy (IRRAS) techniques.

Based on TR-STM measurements, the dynamics of oxidized decanethiol SAMs on Au(111) surfaces were investigated in Chapter 3. The air-oxidized decanethiols arrange in a lamellae-like structure leaving the herringbone reconstruction of the Au(111) surface intact, indicating a rather weak interaction between the molecules and the surface. Successive STM images show that the air-oxidized molecules show less dynamic behaviour compared to the decanethiol molecules. Current-time traces with the feedback loop disabled were recorded at different locations on the surface to probe the dynamic behaviour present on the surface. A two-dimensional activity map of individual current-time traces performed on the decanesulfonate phase reveals that all the dynamics takes place within the vacancy lines. These measurements show that the air-oxidized molecules show less dynamic activity, i.e. lower switching frequency, compared to the regular decanethiol SAM and may be used as a route for creating more robust monolayers. A stochastic two- level switching process is found, however, with a clear preference for one configuration. The I(t) traces provide additional evidence for the proposed models of the various phases and should be considered as fingerprints for the different decanethiol and air-oxidized decanethiol phases found on Au(111).

The restrictive properties of the thiol groups on the SAM applications are the thermal and oxidative instability. The new alternatives to increase the stability of SAMs

have been developed by using different anchoring groups for Au(111) substrate. The direct bond between the carbon and gold consists of the strongest candidate to investigate binding properties, motifs and stability for molecular electronics applications. The terminal alkyne molecules are used to obtain a SAM structure by losing of the terminal hydrogen atom on gold surface. But the main problem of the alkyne groups is that they oxidize during the SAM formation under the ambient conditions. The investigation of the oxidation effect on the SAM formation is the main topic of this chapter. In conclusion, the new oxidation products of the EAEA molecule did not affect the binding properties and the binding is between the carbon atom and Au gold atom of the Au(111) surface. However, we showed that in Chapter 3, the oxidized alkanethiol molecules transform into the sulfonates molecules by physically interacting with the substrate. But oxidized alkyne groups are still chemically bonded between the Au-C which makes these systems very useful for ambient condition applications.

In Chapter 5 we focused our attention on the Ru(II) complex modified CS 28, SAM (on Au(111) substrates). The SAMs were characterized by electrochemical cyclic voltammetry and impedance spectroscopy, STM and XPS methods. The current electrochemical measurements, cyclic voltammetry and impedance spectroscopy, revealed that $Fe(CN)^{3/4-}$ redox reactions on the gold surface are blocked as compared to the bare Au(111) substrate. The defects decrease the resistance of charge transfer of the SAM and allow the access of ions to the substrate. By using the STM and XPS methods, the molecular structure and binding properties of the CS28 molecules were characterized. This provides a deeper insight in the carboxyl and sulfur groups binding affinity to Au(111) substrate. The complex molecule in the monolayer results in a local long-range as observed by STM. The spacing between the parallel stripes is 0.81 nm. There are two possible binding groups, i.e. sulfur and carboxyclic acid groups of the molecule. We found that the sulfur atoms bind to the gold surface. This new SAM system will help us to look for new possibilities and the improvement in applications such as photosensitive molecules, photoactive surfaces and sensors and new photonic application of dye-sensitized solar cell molecules. It will also contribute to a better understanding of the preparation of high quality monolayers.

REFERENCES

Abbott, Nicholas L, Christopher B Gorman, and George M Whitesides. 1995. "Active control of wetting using applied electrical potentials and self-assembled monolayers." *Langmuir* 11 (1):16-18.

Amatore, C, J M_ Savéant, and D Tessier. 1983. "Charge transfer at partially blocked surfaces: a model for the case of microscopic active and inactive sites." *Journal of electroanalytical chemistry and interfacial electrochemistry* 147 (1-2):39-51.

Atesci, Huseyin, Veerabhadrarao Kaliginedi, Jose A Celis Gil, Hiroaki Ozawa, Joseph M Thijssen, Peter Broekmann, Masa-aki Haga, and Sense Jan van der Molen. 2018. "Humidity-controlled rectification switching in ruthenium-complex molecular junctions." *Nature nanotechnology* 13 (2):117.

Bard, Allen J, Larry R Faulkner, Johna Leddy, and Cynthia G Zoski. 1980. *Electrochemical methods: fundamentals and applications*. Vol. 2: wiley New York.

Barriet, David, Chi Ming Yam, Olga E Shmakova, Andrew C Jamison, and T Randall Lee. 2007. "4-mercaptophenylboronic acid SAMs on gold: Comparison with SAMs derived from thiophenol, 4-mercaptophenol, and 4-mercaptobenzoic acid." *Langmuir* 23 (17):8866-8875.

Bejarano, Francesc, Ignacio Jose Olavarria-Contreras, Andrea Droghetti, Ivan Rungger, Alexander Rudnev, Diego Gutiérrez, Marta Mas-Torrent, Jaume Veciana, Herre SJ van der Zant, and Concepció Rovira. 2018. "Robust organic radical molecular junctions using acetylene terminated groups for C-Au bond formation." *Journal of the American Chemical Society*.

Binnig, G., H. Rohrer, Ch Gerber, and E. Weibel. 1982. "Surface Studies by Scanning Tunneling Microscopy." *Physical Review Letters* 49 (1):57-61.

Bliznyuk, Valery N, Mark P Everson, and Vladimir V Tsukruk. 1998. "Nanotribological properties of organic boundary lubricants: Langmuir films versus self-assembled monolayers." *Journal of Tribology* 120 (3):489-495.

Bose, A Chandra, and M Yoshitake. 2005. "Pattern formation induced by Ar+ sputtering on Au (1 1 1)." *Applied surface science* 241 (1-2):174-178.

Bouas-Laurent, Henri, Alain Castellan, Jean-Pierre Desvergne, and René Lapouyade. 2000. "Photodimerization of anthracenes in fluid solution: structural aspects." *Chemical Society Reviews* 29 (1):43-55.

Brown, Treva T, Zorabel M LeJeune, Kai Liu, Sean Hardin, Jie-Ren Li, Kresimir Rupnik, and Jayne C Garno. 2011. "Automated scanning probe lithography with n-alkanethiol self-assembled monolayers on Au (111): Application for teaching

undergraduate laboratories." *JALA: Journal of the Association for Laboratory Automation* 16 (2):112-125.

Bu, Donglei, Thomas J Mullen, and Gang-yu Liu. 2010. "Regulation of local structure and composition of binary disulfide and thiol self-assembled monolayers using nanografting." *ACS nano* 4 (11):6863-6873.

Buchholz, Maria, Mingchun Xu, Heshmat Noei, Peter Weidler, Alexei Nefedov, Karin Fink, Yuemin Wang, and Christof Wöll. 2016. "Interaction of carboxylic acids with rutile TiO2 (110): IR-investigations of terephthalic and benzoic acid adsorbed on a single crystal substrate." *Surface Science* 643:117-123.

Burroughs, John A, and Luke Hanley. 1993. "Laser desorption ion trap mass spectrometry of self-assembled monolayers." *Journal of the American Society for Mass Spectrometry* 4 (12):968-970.

Campuzano, Susana, María Pedrero, Concepción Montemayor, Enrique Fatás, and José M Pingarrón. 2006. "Characterization of alkanethiol-self-assembled monolayers-modified gold electrodes by electrochemical impedance spectroscopy." *Journal of Electroanalytical Chemistry* 586 (1):112-121.

Chaki, Nirmalya K, and K Vijayamohanan. 2002. "Self-assembled monolayers as a tunable platform for biosensor applications." *Biosensors and Bioelectronics* 17 (1):1-12.

Chen, Da, and Jinghong Li. 2006. "Interfacial design and functionization on metal electrodes through self-assembled monolayers." *Surface Science Reports* 61 (11):445-463.

Clegg, Robert S, Scott M Reed, Rachel K Smith, Bridgette L Barron, Jamieson A Rear, and James E Hutchison. 1999. "The interplay of lateral and tiered interactions in stratified self-organized molecular assemblies." *Langmuir* 15 (26):8876-8883.

Collard, David M, and Marye Anne Fox. 1991. "Use of electroactive thiols to study the formation and exchange of alkanethiol monolayers on gold." *Langmuir* 7 (6):1192-1197.

Colton, Richard J. 1998. *Procedures in scanning probe microscopies*: John Wiley & Sons.

Cooper, Elaine, and Graham J Leggett. 1999. "Influence of tail-group hydrogen bonding on the stabilities of self-assembled monolayers of alkylthiols on gold." *Langmuir* 15 (4):1024-1032.

Cortés, Emiliano, Aldo A Rubert, Guillermo Benitez, Pilar Carro, Maria E Vela, and Roberto C Salvarezza. 2009. "Enhanced stability of thiolate self-assembled monolayers (SAMs) on nanostructured gold substrates." *Langmuir* 25 (10):5661-5666.

Crudden, Cathleen M., J. Hugh Horton, Iraklii I. Ebralidze, Olena V. Zenkina, Alastair B. McLean, Benedict Drevniok, Zhe She, Heinz-Bernhard Kraatz, Nicholas J. Mosey, Tomohiro Seki, Eric C. Keske, Joanna D. Leake, Alexander Rousina-Webb, and Gang Wu. 2014. "Ultra stable self-assembled monolayers of N-heterocyclic carbenes on gold." *Nat Chem* 6 (5):409-414.

Deligianni, H. 2010. "Electrochemical Engineering for the 21st Century (Dedicated to Richard C. Alkire)."

Dhirani, Al-Amin, Robert W Zehner, Richard P Hsung, Philippe Guyot-Sionnest, and Lawrence R Sita. 1996. "Self-assembly of conjugated molecular rods: A high-resolution STM study." *Journal of the American Chemical Society* 118 (13):3319-3320.

Diaz, Javier, Guido Paolicelli, Salvador Ferrer, and Fabio Comin. 1996. "Separation of the sp 3 and sp 2 components in the C1s photoemission spectra of amorphous carbon films." *Physical Review B* 54 (11):8064.

Ding, Shinn-Jyh, Bin-Wha Chang, Ching-Chou Wu, Min-Feng Lai, and Hsien-Chang Chang. 2005. "Impedance spectral studies of self-assembly of alkanethiols with different chain lengths using different immobilization strategies on Au electrodes." *Analytica chimica acta* 554 (1-2):43-51.

Dou, Rui-Fen, Xu-Cun Ma, Luan Xi, Hin Lap Yip, King Young Wong, Woon Ming Lau, Jin-Feng Jia, Qi-Kun Xue, Wei-Sheng Yang, and Hong Ma. 2006. "Self-Assembled Monolayers of Aromatic Thiols Stabilized by Parallel-Displaced $\pi-\pi$ Stacking Interactions." *Langmuir* 22 (7):3049-3056.

Du, Xuezhong, Wangen Miao, and Yingqiu Liang. 2005. "IRRAS Studies on Chain Orientation in the Monolayers of Amino Acid Amphiphiles at the Air− Water Interface Depending on Metal Complex and Hydrogen Bond Formation with the Headgroups." *The Journal of Physical Chemistry B* 109 (15):7428-7434.

Eckermann, Amanda L, Daniel J Feld, Justine A Shaw, and Thomas J Meade. 2010. "Electrochemistry of redox-active self-assembled monolayers." *Coordination chemistry reviews* 254 (15-16):1769-1802.

Emberly, Eldon G, and George Kirczenow. 1998. "Theory of electrical conduction through a molecule." *Annals of the New York Academy of Sciences* 852 (1):54-67.

Fenter, P, A Eberhardt, and P Eisenberger. 1994. "Self-assembly of n-alkyl thiols as disulfides on Au (111)." *Science* 266 (5188):1216-1218.

Finklea, H. O., and D. D. Hanshew. 1992. "Electron-transfer kinetics in organized thiol monolayers with attached pentaammine(pyridine)ruthenium redox centers." *Journal of the American Chemical Society* 114 (9):3173-3181.

Fitts, WP, JM White, and GE Poirier. 2002. "Low-coverage decanethiolate structure on Au (111): Substrate effects." *Langmuir* 18 (5):1561-1566.

Folkers, J. P., C. B. Gorman, P. E. Laibinis, S. Buchholz, G. M. Whitesides, and R. G. Nuzzo. 1995. "Self-assembled monolayers of long-chain hydroxamic acids on the native oxides of metals." *Langmuir* 11 (3):813-824.

Fox, HW, EF Hare, and WA Zisman. 1953. "The spreading of liquids on low-energy surfaces. VI. Branched-chain monolayers, aromatic surfaces, and thin liquid films." *Journal of Colloid Science* 8 (2):194-203.

Fox, Marye Anne. 1999. "Fundamentals in the design of molecular electronic devices: Long-range charge carrier transport and electronic coupling." *Accounts of chemical research* 32 (3):201-207.

Fox, Marye Anne, and Marilyn D Wooten. 1997. "Characterization, adsorption, and photochemistry of self-assembled monolayers of 10-thiodecyl 2-anthryl ether on gold." *Langmuir* 13 (26):7099-7105.

Franks, W., S. Tosatti, F. Heer, P. Seif, M. Textor, and A. Hierlemann. 2007. "Patterned cell adhesion by self-assembled structures for use with a CMOS cell-based biosensor." *Biosensors & Bioelectronics* 22 (7):1426-1433.

Fritzsche, J. 1866. "Ueber die festen Kohlenwasserstoffe des Steinkohlentheers." *Journal für Praktische Chemie* 97 (1):290-303.

Fujiwara, Hiroyuki. 2007. *Spectroscopic ellipsometry: principles and applications*: John Wiley & Sons.

Gao, Jianzhi, Juyang Gao, Chao Yan, Mahroo Rokni Fard, Dogan Kaya, Gangqiang Zhu, and Quanmin Guo. 2016. "Growth of Two-Dimensional C60 Nanoclusters within a Propylthiolate Matrix." *The Journal of Physical Chemistry C* 120 (44):25481-25488.

García-Raya, Daniel, Rafael Madueño, José Manuel Sevilla, Manuel Blázquez, and Teresa Pineda. 2008. "Electrochemical characterization of a 1, 8-octanedithiol self-assembled monolayer (ODT-SAM) on a Au (1 1 1) single crystal electrode." *Electrochimica Acta* 53 (27):8026-8033.

Gorbunov, AA, B Wolf, and J Edelmann. 1993. "The use of silver tips in scanning tunneling microscopy." *Review of scientific instruments* 64 (8):2393-2394.

Greenler, Robert G. 1966. "Infrared study of adsorbed molecules on metal surfaces by reflection techniques." *The Journal of Chemical Physics* 44 (1):310-315.

Grönbeck, Henrik, and Michael Odelius. 2010. "Photoemission core-level shifts reveal the thiolate-Au (111) interface." *Physical Review B* 82 (8):085416.

Häkkinen, Hannu. 2012. "The gold-sulfur interface at the nanoscale." *Nature chemistry* 4 (6):443-455.

Hamoudi, Hicham, Zhiang Guo, Mirko Prato, Celine Dablemont, Wan Quan Zheng, Bernard Bourguignon, Maurizio Canepa, and Vladimir A Esaulov. 2008. "On the

self assembly of short chain alkanedithiols." *Physical Chemistry Chemical Physics* 10 (45):6836-6841.

Hanke, Felix, and Jonas Björk. 2013. "Structure and local reactivity of the Au (111) surface reconstruction." *Physical Review B* 87 (23):235422.

Harder, P, M Grunze, R Dahint, GM Whitesides, and PE Laibinis. 1998. "Molecular conformation in oligo (ethylene glycol)-terminated self-assembled monolayers on gold and silver surfaces determines their ability to resist protein adsorption." *The Journal of Physical Chemistry B* 102 (2):426-436.

Harris, Jeremy J, and Merlin L Bruening. 2000. "Electrochemical and in situ ellipsometric investigation of the permeability and stability of layered polyelectrolyte films." *Langmuir* 16 (4):2006-2013.

Hauptmann, Nadine, Christian Hamann, Hao Tang, and Richard Berndt. 2013. "Soft-landing electrospray deposition of the ruthenium dye N3 on Au (111)." *The Journal of Physical Chemistry C* 117 (19):9734-9738.

Hay, JM, and D Lyon. 1970. "Alkyne oxidation I. Acetylene oxidation." *Proc. R. Soc. Lond. A* 317 (1528):1-20.

Hong, Wenjing, Hui Li, Shi-Xia Liu, Yongchun Fu, Jianfeng Li, Veerabhadrarao Kaliginedi, Silvio Decurtins, and Thomas Wandlowski. 2012. "Trimethylsilyl-terminated oligo (phenylene ethynylene) s: an approach to single-molecule junctions with covalent Au–C σ-bonds." *Journal of the American Chemical Society* 134 (47):19425-19431.

Hutt, David A, Elaine Cooper, and Graham J Leggett. 1998. "Structure and mechanism of photooxidation of self-assembled monolayers of alkylthiols on silver studied by XPS and static SIMS." *The Journal of Physical Chemistry B* 102 (1):174-184.

Hutt, David A, and Graham J Leggett. 1996. "Influence of adsorbate ordering on rates of UV photooxidation of self-assembled monolayers." *The Journal of Physical Chemistry* 100 (16):6657-6662.

Jakhmola, Anshuman, M Celentano, R Vecchione, A Manikas, E Battista, V Calcagno, and PA Netti. 2017. "Self-assembly of gold nanowire networks into gold foams: production, ultrastructure and applications." *Inorganic Chemistry Frontiers* 4 (6):1033-1041.

Jennings, G. K., and P. E. Laibinis. 1996. "Self-assembled monolayers of alkanethiols on copper provide corrosion resistance in aqueous environments." *Colloids and Surfaces a-Physicochemical and Engineering Aspects* 116 (1-2):105-114.

Jewell, A. D., H. L. Tierney, and E. C. H. Sykes. 2010a. "Gently lifting gold's herringbone reconstruction: Trimethylphosphine on Au(111)." *Physical Review B* 82 (20):6.

Jewell, April D, Samuel J Kyran, Daniel Rabinovich, and E Charles H Sykes. 2012. "Effect of Head-Group Chemistry on Surface-Mediated Molecular Self-Assembly." *Chemistry-A European Journal* 18 (23):7169-7178.

Jewell, April D, Heather L Tierney, and E Charles H Sykes. 2010b. "Gently lifting Gold's herringbone reconstruction: trimethylphosphine on Au (111)." *Physical Review B* 82 (20):205401.

Ju, Bing-Feng, Yuan-Liu Chen, and Yaozheng Ge. 2011. "The art of electrochemical etching for preparing tungsten probes with controllable tip profile and characteristic parameters." *Review of Scientific Instruments* 82 (1):013707.

Käfer, Daniel, Gregor Witte, Piotr Cyganik, Andreas Terfort, and Christof Wöll. 2006. "A comprehensive study of self-assembled monolayers of anthracenethiol on gold: Solvent effects, structure, and stability." *Journal of the American Chemical Society* 128 (5):1723-1732.

Kang, Xiongwu, Nathaniel B Zuckerman, Joseph P Konopelski, and Shaowei Chen. 2012. "Alkyne-functionalized ruthenium nanoparticles: ruthenium–vinylidene bonds at the metal–ligand interface." *Journal of the American Chemical Society* 134 (3):1412-1415.

Katsonis, Nathalie, Alexandr Marchenko, Sébastien Taillemite, Denis Fichou, Gaëlle Chouraqui, Corinne Aubert, and Max Malacria. 2003. "A Molecular Approach to Self-Assembly of Trimethylsilylacetylene Derivatives on Gold." *Chemistry-A European Journal* 9 (11):2574-2581.

Kessel, Carl R, and Steve Granick. 1991. "Formation and characterization of a highly ordered and well-anchored alkylsilane monolayer on mica by self-assembly." *Langmuir* 7 (3):532-538.

Kockmann, Daan, Bene Poelsema, and Harold JW Zandvliet. 2009. "Transport through a single octanethiol molecule." *Nano letters* 9 (3):1147-1151.

Kutsenko, VY, YY Lopatina, Léo Bossard-Giannesini, OA Marchenko, Olivier Pluchery, and SV Snegir. 2017. "Alkylthiol self-assembled monolayers on Au (111) with tailored tail groups for attaching gold nanoparticles." *Nanotechnology* 28 (23):235603.

Laibinis, Paul E, George M Whitesides, David L Allara, Yu Tai Tao, Atul N Parikh, and Ralph G Nuzzo. 1991. "Comparison of the structures and wetting properties of self-assembled monolayers of n-alkanethiols on the coinage metal surfaces, copper, silver, and gold." *Journal of the American Chemical Society* 113 (19):7152-7167.

Lewis, Mary, Michael Tarlov, and Keith Carron. 1995. "Study of the photooxidation process of self-assembled alkanethiol monolayers." *Journal of the American Chemical Society* 117 (37):9574-9575.

Li, Shan-Shan, Li-Ping Xu, Li-Jun Wan, Shu-Tao Wang, and Lei Jiang. 2006. "Time-dependent organization and wettability of decanethiol self-assembled monolayer on Au (111) investigated with STM." *The Journal of Physical Chemistry B* 110 (4):1794-1799.

Li, Wenxin, Grant G Langlois, Natalie A Kautz, and SJ Sibener. 2014. "Formation of Stabilized Ketene Intermediates in the Reaction of O (3P) with Oligo (phenylene ethynylene) Thiolate Self-Assembled Monolayers on Au (111)." *The Journal of Physical Chemistry C* 118 (29):15846-15852.

Lin, S., and R. L. McCarley. 1999. "Surface-confined monomers on electrode surfaces. 6. Adsorption and polymerization of 1,6-diisocyanohexane on Au and Pt." *Langmuir* 15 (1):151-159.

Love, J Christopher, Lara A Estroff, Jennah K Kriebel, Ralph G Nuzzo, and George M Whitesides. 2005. "Self-assembled monolayers of thiolates on metals as a form of nanotechnology." *Chemical reviews* 105 (4):1103-1170.

Maity, Prasenjit, Shinjiro Takano, Seiji Yamazoe, Tomonari Wakabayashi, and Tatsuya Tsukuda. 2013. "Binding motif of terminal alkynes on gold clusters." *Journal of the American Chemical Society* 135 (25):9450-9457.

Maksymovych, Peter, Dan C Sorescu, and John T Yates Jr. 2006. "Gold-adatom-mediated bonding in self-assembled short-chain alkanethiolate species on the Au (111) surface." *Physical review letters* 97 (14):146103.

Mamun, Abdulla Hel Al, and Jae Ryang Hahn. 2012. "Effects of Solvent on the Formation of Octanethiol Self-Assembled Monolayers on Au (111) at High Temperatures in a Closed Vessel: A Scanning Tunneling Microscopy and X-ray Photoelectron Spectroscopy Study." *The Journal of Physical Chemistry C* 116 (42):22441-22448.

Mayor, Louise C, Alex Saywell, Graziano Magnano, Christopher J Satterley, Joachim Schnadt, and James N O'Shea. 2009. "Adsorption of a Ru (II) dye complex on the Au (111) surface: Photoemission and scanning tunneling microscopy." *The Journal of chemical physics* 130 (16):164704.

McDonagh, Andrew M, Hadi M Zareie, Michael J Ford, Christopher S Barton, Milena Ginic-Markovic, and Janis G Matisons. 2007. "Ethynylbenzene monolayers on gold: a metal-molecule binding motif derived from a hydrocarbon." *Journal of the American Chemical Society* 129 (12):3533-3538.

McFarland, Eric W, and Jing Tang. 2003. "A photovoltaic device structure based on internal electron emission." *Nature* 421 (6923):616.

Mendes, Renata K, Renato S Freire, Carla P Fonseca, Silmara Neves, and Lauro T Kubota. 2004. "Characterization of self-assembled thiols monolayers on gold surface by electrochemical impedance spectroscopy." *Journal of the Brazilian Chemical Society* 15 (6):849-855.

Nerngchamnong, Nisachol, Hairong Wu, Kai Sotthewes, Li Yuan, Liang Cao, Max Roemer, Jiong Lu, Kian Ping Loh, Cedric Troadec, and Harold JW Zandvliet. 2014. "Supramolecular structure of self-assembled monolayers of ferrocenyl terminated n-alkanethiolates on gold surfaces." *Langmuir* 30 (44):13447-13455.

Nguyen, Van Quynh, Xiaonan Sun, Frédéric Lafolet, Jean-Frédéric Audibert, Fabien Miomandre, Gilles Lemercier, Frédérique Loiseau, and Jean-Christophe Lacroix. 2016. "Unprecedented self-organized monolayer of a Ru (II) complex by diazonium electroreduction." *Journal of the American Chemical Society* 138 (30):9381-9384.

Nicholson, Richard Selindh, and Irving Shain. 1964. "Theory of stationary electrode polarography. Single scan and cyclic methods applied to reversible, irreversible, and kinetic systems." *Analytical Chemistry* 36 (4):706-723.

Nielsen, Michael H, and Jonathan RI Lee. 2013. "Preparation of Organothiol Self-Assembled Monolayers for Use in Templated Crystallization." In *Methods in enzymology*, 209-224. Elsevier.

Nilsson, Daniel, Somsakul Watcharinyanon, Mattias Eng, Liqian Li, Ellen Moons, Lars SO Johansson, Michael Zharnikov, Andrey Shaporenko, Bo Albinsson, and Jerker Mårtensson. 2007. "Characterization of self-assembled monolayers of oligo (phenyleneethynylene) derivatives of varying shapes on gold: Effect of laterally extended π-systems." *Langmuir* 23 (11):6170-6181.

Noh, Jaegeun, and Masahiko Hara. 2000. "Nanoscopic evidence for dissociative adsorption of asymmetric disulfide self-assembled monolayers on Au (111)." *Langmuir* 16 (5):2045-2048.

Noh, Jaegeun, and Masahiko Hara. 2001. "Molecular-scale desorption processes and the alternating missing-row phase of alkanethiol self-assembled monolayers on Au (111)." *Langmuir* 17 (23):7280-7285.

Noh, Jaegeun, Hiroyuki S Kato, Maki Kawai, and Masahiko Hara. 2006. "Surface structure and interface dynamics of alkanethiol self-assembled monolayers on Au (111)." *The Journal of Physical Chemistry B* 110 (6):2793-2797.

Palegrosdemange, C., E. S. Simon, K. L. Prime, and G. M. Whitesides. 1991. "Formation of self-assembled monolayers by chemisorption of derivatives of oligo(ethylene glycol) of structure hs(ch2)11(och2ch2)meta-oh on gold." *Journal of the American Chemical Society* 113 (1):12-20.

Parrish, Jonathan D, Michael A Ischay, Zhan Lu, Song Guo, Noël R Peters, and Tehshik P Yoon. 2012. "Endoperoxide synthesis by photocatalytic aerobic [2+ 2+ 2] cycloadditions." *Organic letters* 14 (6):1640-1643.

Passaglia, Elio, Robert R Stromberg, and Jerome Kruger. 1964. *Ellipsometry in the Measurement of Surfaces and Thin Films: Symposium Proceedings*. Vol. 256: US National Bureau of Standards.

Paul Pijpers, A, and Robert J. Meier. 1999. "Core level photoelectron spectroscopy for polymer and catalyst characterisation." *Chemical Society Reviews* 28 (4):233-238.

Pissinis, Diego E, Omar E Linarez Pérez, Fernando P Cometto, and Manuel López Teijelo. 2014. "Preparation and characterization of self assembled monolayers of 2-mercaptonicotinic acid on Au (1 1 1)." *Journal of Electroanalytical Chemistry* 712:167-177.

Pla-Vilanova, Pepita, Albert C Aragonès, Simone Ciampi, Fausto Sanz, Nadim Darwish, and Ismael Diez-Perez. 2015. "The spontaneous formation of single-molecule junctions via terminal alkynes." *Nanotechnology* 26 (38):381001.

Pletincx, Sven, Lena Trotochaud, Laura-Lynn Fockaert, Johannes MC Mol, Ashley R Head, Osman Karslıoğlu, Hendrik Bluhm, Herman Terryn, and Tom Hauffman. 2017. "In situ characterization of the initial effect of water on molecular interactions at the interface of organic/inorganic hybrid systems." *Scientific reports* 7:45123.

Poirier, GE. 1999. "Coverage-dependent phases and phase stability of decanethiol on Au (111)." *Langmuir* 15 (4):1167-1175.

Poirier, GE, WP Fitts, and JM White. 2001. "Two-dimensional phase diagram of decanethiol on Au (111)." *Langmuir* 17 (4):1176-1183.

Poirier, Gregory E, Tonya M Herne, C Cameron Miller, and Michael J Tarlov. 1999. "Molecular-scale characterization of the reaction of ozone with decanethiol monolayers on Au (111)." *Journal of the American Chemical Society* 121 (41):9703-9711.

Pritzkow, Wilhelm, and Tarigopula Siva Sankara Rao. 1985. "Studies on the Autoxidation of Phenylacetylene." *Advanced Synthesis & Catalysis* 327 (6):887-892.

Qian, Yile, Guohua Yang, Jingjiang Yu, Thomas A Jung, and Gang-yu Liu. 2003. "Structures of annealed decanethiol self-assembled monolayers on Au (111): an ultrahigh vacuum scanning tunneling microscopy study." *Langmuir* 19 (15):6056-6065.

Rajalingam, K, L Hallmann, T Strunskus, A Bashir, C Wöll, and F Tuczek. 2010. "Self-assembled monolayers of benzylmercaptan and para-cyanobenzylmercaptan on gold: surface infrared spectroscopic characterization." *Physical Chemistry Chemical Physics* 12 (17):4390-4399.

Ramin, Michaël A, Gwénaëlle Le Bourdon, Nicolas Daugey, Bernard Bennetau, Luc Vellutini, and Thierry Buffeteau. 2011. "PM-IRRAS investigation of self-assembled monolayers grafted onto SiO2/Au substrates." *Langmuir* 27 (10):6076-6084.

Rogers, BL, JG Shapter, WM Skinner, and K Gascoigne. 2000. "A method for production of cheap, reliable pt–ir tips." *Review of Scientific Instruments* 71 (4):1702-1705.

Rogers, Nicola J, Sunil Claire, Robert M Harris, Shiva Farabi, Gerald Zikeli, Iain B Styles, Nikolas J Hodges, and Zoe Pikramenou. 2014. "High coating of Ru (II) complexes on gold nanoparticles for single particle luminescence imaging in cells." *Chemical Communications* 50 (5):617-619.

Ron, Hannoch, Sophie Matlis, and Israel Rubinstein. 1998. "Self-assembled monolayers on oxidized metals. 2. Gold surface oxidative pretreatment, monolayer properties, and depression formation." *Langmuir* 14 (5):1116-1121.

Roncali, P, E Tavitian, B Texier, O Peltie, F Perrault, J Boutet, L Cognet, B Lounis, D Marguet, and O Thoumine. 2010. "Nanoscience Nanobiotechnology and Nanobiology." *P. Boisseau, P. Houdy, M. Lahmani (Eds.)*.

Rossel, Frédéric, Pierre Brodard, François Patthey, Neville V Richardson, and Wolf-Dieter Schneider. 2008. "Modified herringbone reconstruction on Au (111) induced by self-assembled Azure A islands." *Surface Science* 602 (14):L115-L117.

San Juan, Ronan Roca. 2013. "Self-Assembled Monolayers of Dithiophosphinic Acids on Gold."

Schaffert, Johannes, Maren C Cottin, Andreas Sonntag, Hatice Karacuban, Christian A Bobisch, Nicolás Lorente, Jean-Pierre Gauyacq, and Rolf Möller. 2013. "Imaging the dynamics of individually adsorbed molecules." *Nature materials* 12 (3):223-227.

Schnadt, Joachim, Paul A Brühwiler, Luc Patthey, James N O'shea, Sven Södergren, Michael Odelius, Rajeev Ahuja, Olof Karis, Margit Bässler, and Petter Persson. 2002. "Experimental evidence for sub-3-fs charge transfer from an aromatic adsorbate to a semiconductor." *Nature* 418 (6898):620.

Schoenfisch, Mark H, and Jeanne E Pemberton. 1998. "Air stability of alkanethiol self-assembled monolayers on silver and gold surfaces." *Journal of the American Chemical Society* 120 (18):4502-4513.

Senaratne, Wageesha, Luisa Andruzzi, and Christopher K Ober. 2005. "Self-assembled monolayers and polymer brushes in biotechnology: current applications and future perspectives." *Biomacromolecules* 6 (5):2427-2448.

Setvín, M, J Javorský, D Turčinková, I Matolínová, P Sobotík, P Kocán, and I Ošt'ádal. 2012. "Ultrasharp tungsten tips—characterization and nondestructive cleaning." *Ultramicroscopy* 113:152-157.

Shi, Zheng. 2013. "Electrical, Optical And Chemical Properties Of Organic Photo Sensitve Materials."

Smith, Tennyson. 1980. "The hydrophilic nature of a clean gold surface." *Journal of Colloid and Interface Science* 75 (1):51-55.

Sohn, Y, W Wei, and JM White. 2007. "Phenylacetylene on Cu (111): Adsorption geometry, interfacial electronic structures and thermal chemistry." *The Journal of Physical Chemistry C* 111 (13):5101-5110.

Song, Yong, Rahul Premachandran Nair, Min Zou, and Yongqiang Wang. 2009. "Superhydrophobic surfaces produced by applying a self-assembled monolayer to silicon micro/nano-textured surfaces." *Nano Research* 2 (2):143-150.

Sotthewes, Kai, Victor Geskin, René Heimbuch, Avijit Kumar, and Harold JW Zandvliet. 2014. "Research update: molecular electronics: the single-molecule switch and transistor." *APL materials* 2 (1):010701.

Sotthewes, Kai, Rene Heimbuch, and Henricus JW Zandvliet. 2015. "Dynamics of copper-phthalocyanine molecules on Au/Ge (001)." *The Journal of chemical physics* 143 (13):134303.

Sotthewes, Kai, Özlem Kap, Hairong Wu, Damien Thompson, Jurriaan Huskens, and Harold J. W. Zandvliet. 2018. "Ordering of Air-Oxidized Decanethiols on Au(111)." *The Journal of Physical Chemistry C* 122 (15):8430-8436.

Sotthewes, Kai, Hairong Wu, Avijit Kumar, G Julius Vancso, Peter M Schön, and Harold JW Zandvliet. 2013. "Molecular Dynamics and Energy Landscape of Decanethiolates in Self-Assembled Monolayers on Au (111) Studied by Scanning Tunneling Microscopy." *Langmuir* 29 (11):3662-3667.

Srisombat, Laongnuan, Andrew C Jamison, and T Randall Lee. 2011. "Stability: A key issue for self-assembled monolayers on gold as thin-film coatings and nanoparticle protectants." *Colloids and Surfaces A: Physicochemical and Engineering Aspects* 390 (1):1-19.

Steiner, U. B., W. R. Caseri, and U. W. Suter. 1992. "Adsorption of alkanenitriles and alkanedinitriles on gold and copper." *Langmuir* 8 (11):2771-2777.

Stipe, BC, MA Rezaei, W Ho, S Gao, M Persson, and BI Lundqvist. 1997. "Single-molecule dissociation by tunneling electrons." *Physical review letters* 78 (23):4410.

Sun, Lanlan, Yuri A Diaz-Fernandez, Tina A Gschneidtner, Fredrik Westerlund, Samuel Lara-Avila, and Kasper Moth-Poulsen. 2014. "Single-molecule electronics: from chemical design to functional devices." *Chemical Society Reviews* 43 (21):7378-7411.

Sygkridou, D, C Sahin, C Varlikli, and E Stathatos. 2015. "Comparative studies of pyridine and bipyridine ruthenium dye complexes with different side groups as sensitizers in sol-gel quasi-solid-state dye sensitized solar cells." *Electrochimica Acta* 160:227-234.

Tang, Qing, and De-en Jiang. 2014. "Insights into the PhC≡C/Au Interface." *The Journal of Physical Chemistry C* 119 (20):10804-10810.

Tarlov, Michael J, and John G Newman. 1992. "Static secondary ion mass spectrometry of self-assembled alkanethiol monolayers on gold." *Langmuir* 8 (5):1398-1405.

Toerker, M, R Staub, T Fritz, T Schmitz-Hübsch, F Sellam, and K Leo. 2000. "Annealed decanethiol monolayers on Au (111)–intermediate phases between structures with high and low molecular surface density." *Surface science* 445 (1):100-108.

Tour, James M, LeRoy Jones, Darren L Pearson, Jaydeep JS Lamba, Timothy P Burgin, George M Whitesides, David L Allara, Atul N Parikh, and Sundar Atre. 1995. "Self-assembled monolayers and multilayers of conjugated thiols,. alpha.,. omega.-dithiols, and thioacetyl-containing adsorbates. Understanding attachments between potential molecular wires and gold surfaces." *Journal of the American Chemical Society* 117 (37):9529-9534.

Tour, JM. 2003. Ц Molecular Electronics: Commercial In sights, Chemistry, Devices, Architecture and Program ming. Singapore: Wforld Scientific Publishing Co. Pte. Ltd.

Toyota, Shinji. 2010. "Rotational isomerism involving acetylene carbon." *Chemical reviews* 110 (9):5398-5424.

Ulman, Abraham. 1996. "Formation and structure of self-assembled monolayers." *Chemical reviews* 96 (4):1533-1554.

Ulman, Abraham. 2013. *An Introduction to Ultrathin Organic Films: From Langmuir--Blodgett to Self--Assembly*: Academic press.

Uosaki, Kohei, Ye Shen, and Toshihiro Kondo. 1995. "Preparation of a highly ordered Au (111) phase on a polycrystalline gold substrate by vacuum deposition and its characterization by XRD, GISXRD, STM/AFM, and electrochemical measurements." *The Journal of physical chemistry* 99 (38):14117-14122.

Vericat, C, ME Vela, G Benitez, P Carro, and RC Salvarezza. 2010. "Self-assembled monolayers of thiols and dithiols on gold: new challenges for a well-known system." *Chemical Society Reviews* 39 (5):1805-1834.

Vericat, C, ME Vela, and RC Salvarezza. 2005. "Self-assembled monolayers of alkanethiols on Au (111): surface structures, defects and dynamics." *Physical Chemistry Chemical Physics* 7 (18):3258-3268.

Vericat, Carolina, Maria Elena Vela, Gastón Corthey, E Pensa, E Cortés, Mariano Hernan Fonticelli, F Ibanez, GE Benitez, P Carro, and Roberto Carlos Salvarezza. 2014. "Self-assembled monolayers of thiolates on metals: a review article on sulfur-metal chemistry and surface structures." *RSC Advances* 4 (53):27730-27754.

Vesel, Alenka, Aleksander Drenik, Rok Zaplotnik, Miran Mozetic, and Marianne Balat-Pichelin. 2010. "Reduction of thin oxide films on tungsten substrate with highly

reactive cold hydrogen plasma." *Surface and Interface Analysis* 42 (6-7):1168-1171.

Vollhardt, K Peter C, and Neil E Schore. 2014. *Organic Chemistry; Palgrave version: Structure and Function*: Palgrave Macmillan.

Wang, Zhengjia, Jiahao Chen, Stephanie Oyola-Reynoso, and Martin Thuo. 2015. "The Porter-Whitesides Discrepancy: Revisiting Odd-Even Effects in Wetting Properties of n-Alkanethiolate SAMs." *Coatings* 5 (4):1034-1055.

Wasserman, Harry H, Kenneth B Wiberg, David L Larsen, and Jonathan Parr. 2005. "Photooxidation of methylnaphthalenes." *The Journal of organic chemistry* 70 (1):105-109.

Wasserman, Stephen R, George M Whitesides, Ian M Tidswell, Ben M Ocko, Peter S Pershan, and John D Axe. 1989. "The structure of self-assembled monolayers of alkylsiloxanes on silicon: a comparison of results from ellipsometry and low-angle x-ray reflectivity." *Journal of the American Chemical Society* 111 (15):5852-5861.

Whelan, Caroline M, Jacques Ghijsen, Jean-Jacques Pireaux, and Karen Maex. 2004. "Cu adsorption on carboxylic acid-terminated self-assembled monolayers: a high-resolution X-ray photoelectron spectroscopy study." *Thin Solid Films* 464:388-392.

Wiesendanger, Roland. 1994. *Scanning probe microscopy and spectroscopy: methods and applications*: Cambridge University Press.

Willey, Trevor M, Andrew L Vance, T Van Buuren, C Bostedt, LJ Terminello, and CS Fadley. 2005. "Rapid degradation of alkanethiol-based self-assembled monolayers on gold in ambient laboratory conditions." *Surface Science* 576 (1):188-196.

Wöll, Ch, S Chiang, RJ Wilson, and PH Lippel. 1989. "Determination of atom positions at stacking-fault dislocations on Au (111) by scanning tunneling microscopy." *Physical Review B* 39 (11):7988.

Wu, Hairong, Kai Sotthewes, Avijit Kumar, G Julius Vancso, Peter M Schön, and Harold JW Zandvliet. 2013. "Dynamics of decanethiol self-Assembled monolayers on Au (111) studied by time-Resolved Scanning Tunneling Microscopy." *Langmuir* 29 (7):2250-2257.

Wu, Hairong, Kai Sotthewes, Peter M Schön, G Julius Vancso, and Harold JW Zandvliet. 2015. "Ordering and dynamics of oligo (phenylene ethynylene) self-assembled monolayers on Au (111)." *RSC advances* 5 (52):42069-42074.

Yang, Guohua, and Gang-yu Liu. 2003. New insights for self-assembled monolayers of organothiols on Au (111) revealed by scanning tunneling microscopy. ACS Publications.

Yang, Zhongping, Araceli Gonzalez-Cortes, Gilles Jourquin, Jean-Claude Vire, Jean-Michel Kauffmann, and Jean-Luc Delplancke. 1995. "Analytical application of self assembled monolayers on gold electrodes: critical importance of surface pretreatment." *Biosensors and Bioelectronics* 10 (9-10):789-795.

Zaba, Tomasz, Agnieszka Noworolska, Carleen Morris Bowers, Benjamin Breiten, George M Whitesides, and Piotr Cyganik. 2014. "Formation of highly ordered self-assembled monolayers of alkynes on Au (111) substrate." *Journal of the American Chemical Society* 136 (34):11918-11921.

Zareie, M Hadi, Jeffrey Barber, and Andrew M McDonagh. 2006. "Structural changes in self-assembled monolayers initiated by ultraviolet light." *The Journal of Physical Chemistry B* 110 (32):15951-15954.

Zeng, Changgan, Bin Li, Bing Wang, Haiqian Wang, Kedong Wang, Jinlong Yang, JG Hou, and Qingshi Zhu. 2002. "What can a scanning tunneling microscope image do for the insulating alkanethiol molecules on Au (111) substrates?" *The Journal of chemical physics* 117 (2):851-856.

Zhang, Liming. 2014. "A non-diazo approach to α-oxo gold carbenes via gold-catalyzed alkyne oxidation." *Accounts of chemical research* 47 (3):877-888.

Zhang, Luzheng, William A Goddard III, and Shaoyi Jiang. 2002. "Molecular simulation study of the c (4× 2) superlattice structure of alkanethiol self-assembled monolayers on Au (111)." *The Journal of chemical physics* 117 (15):7342-7349.

Zhang, Sheng, Kusum L Chandra, and Christopher B Gorman. 2007. "Self-assembled monolayers of terminal alkynes on gold." *Journal of the American Chemical Society* 129 (16):4876-4877.

Zhang, Yi-Qi, Nenad Kepčija, Martin Kleinschrodt, Katharina Diller, Sybille Fischer, Anthoula C Papageorgiou, Francesco Allegretti, Jonas Björk, Svetlana Klyatskaya, and Florian Klappenberger. 2012. "Homo-coupling of terminal alkynes on a noble metal surface." *Nature communications* 3:1286.

Zhao, P, CF Fang, CJ Xia, YM Wang, DS Liu, and SJ Xie. 2008. "A possible anthracene-based optical molecular switch driven by a reversible photodimerization reaction." *Applied Physics Letters* 93 (1):013113.

VITA

PERSONAL INFORMATION

Surname, Name: KAP OZLEM
Nationality: Turkish (TC)
Date and Place of Birth: 04.06.1986, ELAZIĞ
Phone: +90 (535) 3642933
E-mail: ozzkap@gmail.com

EDUCATION

Degree Institution Year of Graduation
MSc Ege University 2012
BSc Ege University 2010

PUBLICATIONS

Kap Ö., Sotthewes K., Varlıklı C., Zandvliet H., 'Structural dynamics of air-oxidized decanethiols using time-resolved stm' *In progress*

Kap Ö., Şahin Ç., Sotthewes K., Patil P., Zandvliet H., Varlıklı C., 'Molecular structure and binding properties of self-organized monolayer: a ruthenium(II) dye complex on Au(111)' *In progress*

Kap Ö, Sotthewes K., Üçüncü M., Varlıklı C., Zandvliet H., Zareie H., **'**Oxidation of anthracene based alkyne ligand molecule on Au (111)' *In progress*

Sotthewes K., Kap Ö. Wu H., Thompson D., Huskens J., Zandvliet H., 'Ordering of air-oxidized decanethiolate on Au(111)'. Journal of Physical Chemistry C, 2018, DOI: 10.1021/acs.jpcc.8b01389

Horzum N., Kap Ö., Farzaneh A., 'Superhydrophobicity of polystyrene/SiO_2 nanocomposite via electrospining method on Magnesium AZ31 alloy.' Turkish Journal of Chemistry, 2018, DOI: 10.3906/kim-1711-22